NRL/FR/5554--93-9575

Northern Exposure 92: An Investigation of Transauroral HF Radio Skywave Propagation

LEONARD S. WAGNER
JOSEPH A. GOLDSTEIN
MICHAEL A. RUPAR
EDWARD J. KENNEDY

Transmission Technology Branch
Information Technology Division

September 29, 1993

REPORT DOCUMENTATION PAGE

Form Approved
OMB No. 0704-0188

1. AGENCY USE ONLY (*Leave Blank*)	2. REPORT DATE	3. REPORT TYPE AND DATES COVERED
	September 29, 1993	Interim Report (continuing program)

4. TITLE AND SUBTITLE

Northern Exposure 92: An Investigation of Transauroral HF Radio Skywave Propagation

5. FUNDING NUMBERS

PE - 61153N33
PR - LR0330244
TA - 033-02-44
WU - 3410-00

6. AUTHOR(S)

Leonard S. Wagner, Joseph A. Goldstein, Michael A. Rupar, and Edward J. Kennedy

7. PERFORMING ORGANIZATION NAME(S) AND ADDRESS(ES)

Naval Research Laboratory
Washington, DC 20375-5320

8. PERFORMING ORGANIZATION REPORT NUMBER

NRL/FR/5554--93-9575

9. SPONSORING/MONITORING AGENCY NAME(S) AND ADDRESS(ES)

Office of Naval Research
Arlington, VA 22217-5660

10. SPONSORING/MONITORING AGENCY REPORT NUMBER

11. SUPPLEMENTARY NOTES

12a. DISTRIBUTION/AVAILABILITY STATEMENT

Approved for public release; distribution unlimited.

12b. DISTRIBUTION CODE

13. ABSTRACT (*Maximum 200 words*)

The primary objective of the Northern Exposure 92 campaign was to assist in the evaluation of the performance capabilities of a wideband, high frequency, Rake radio receiver on a transauroral skywave channel. A review of the data collected on the transauroral channel during the Northern Exposure 92 exercises indicates that one is likely to encounter three types of signals on the channel: (1) a strong, specularly reflected signal characterized by the usual ionospheric dispersive delay spread and negligible Doppler spread, (2) strong specular multipath signals, exhibiting extensive delay and Doppler spread, and (3) weak scatter signals, exhibiting the widest delay and Doppler spreads. The nonspread reflected signals are encountered during magnetically quiet, daytime conditions where the ionosphere may be described as laminar. The strong, specular-multipath signals occur mostly at night and are associated with reflections from large scale irregularities of electron density characterized by strong horizontal gradients capable of "reflecting" signals whose frequencies lie below some equivalent "maximum usable frequency" (MUF) defined by the path, the background ionosphere, and the maximum electron density in the irregularity region. The weak scattered signals occur at night and are associated with volume scatter from the irregular medium. The scattered signals present the greatest challenge to communication systems with amplitudes $\sim$30 dB less than those of reflected signals and with 2σ Doppler spreads as large as 30 Hz.

14. SUBJECT TERMS

HF skywave
Propagation
Wideband communications
Pulse sounder
Channel characterization

15. NUMBER OF PAGES

53

16. PRICE CODE

17. SECURITY CLASSIFICATION OF REPORT	18. SECURITY CLASSIFICATION OF THIS PAGE	19. SECURITY CLASSIFICATION OF ABSTRACT	20. LIMITATION OF ABSTRACT
UNCLASSIFIED	UNCLASSIFIED	UNCLASSIFIED	UL

NSN 7540-01-280-5500

Standard Form 298 (Rev. 2-89)
Prescribed by ANSI Std 239-18
298-102

CONTENTS

EXECUTIVE SUMMARY

As a result of recent developments in spread spectrum methods and VLSI technology, the "Rake" technique (Price and Green, 1958) now appears to be a practical option for dealing with performance problems associated with disturbed ionospheric conditions on the high-frequency skywave radio channel. The effectiveness of this technique depends on the extent of the dispersive delay spread and on the time rate of change of the channel characteristics (as measured by the signal Doppler spread) relative to the adaptive rate of the Rake.

The primary objective of the Northern Exposure 92 campaign was to explore the performance capabilities of a WBHF-Rake on the transauroral skywave channel. The transauroral channel is probably the most difficult of all skywave channels because of the frequent and unpredictable nature of intense ionospheric disturbance conditions on the channel. For meaningful results, any communication test must be accompanied by simultaneous measurements of the channel characteristics. In pursuit of that goal, NRL and the Raytheon Corporation and Mitre Corporation undertook joint measurements on radio links involving transmission via the auroral ionosphere.

A secondary objective of the Northern Exposure measurement series was to add to the existing database of transauroral measurements. An estimate of the performance improvement that can be achieved by using modern wideband Rake techniques depends on an accurate knowledge of the range of conditions that can be expected on the channel. Published reports of the characteristics of the transauroral channel are not extensive and are limited to periods around solar minimum, when the monthly mean smoothed sunspot number was ~15. The particular importance of Northern Exposure 92 measurements lies in the fact that they apply to a time period that follows the most recent solar maximum. The measurements reported here were taken during the period between 13 March and 2 April 1992, which was approximately two years after the peak of the current solar cycle (cycle #22). Magnetic conditions during the measurement period were "unsettled" to "active" and the mean sunspot number for the period was 108. This compares with a maximum observed sunspot number of 158 during June and July of 1989 and a value of 124 during January of 1992, just before the measurement period.

The propagation path chosen for the Northern Exposure measurements was between Sondrestrom, Greenland and Keflavik, Iceland. This path was selected because it provides a one hop propagation path of moderate range (~1300 km) with a nighttime midpath point that lies within the auroral zone under all conditions of geomagnetic disturbance. During the daytime, the midpath point for this path can be shown to be subauroral for all conditions except those related to a major magnetic storm. The time interval about local noon for which the midpath point is subauroral gradually diminishes as the level of magnetic disturbance increases from quiet to storm-time conditions.

A review of the data collected on the transauroral channel during the Northern Exposure 92 exercises indicates that one is likely to encounter three types of signals on the channel: (1) a strong, specularly reflected signal characterized by the usual ionospheric dispersive delay spread and negligible Doppler spread, (2) strong specular-multipath signals, exhibiting extensive delay and Doppler spread, and (3) weak scatter signals, exhibiting the widest delay and Doppler spreads. The nonspread reflected signals are encountered during magnetically quiet, daytime conditions where the ionosphere may be

described as laminar. The strong, specular-multipath signals occur mostly at night and are associated with reflections from large scale irregularities of electron density characterized by strong horizontal gradients capable of "reflecting" signals whose frequencies lie below some equivalent "maximum usable frequency" (MUF) defined by the path, the background ionosphere, and the maximum electron density in the irregularity region. The weak scattered signals occur at night and are associated with volume scatter from the irregular medium. The scattered signals present the greatest challenge to communication systems with amplitudes ~30 dB less than those of reflected signals and with 2σ Doppler spreads as large as 30 Hz.

The broad delay and Doppler spreads observed at night are attributable to reflection and/or scatter from highly anisotropic field aligned irregularities of electron density that are a persistent feature of the nighttime auroral F layer. Measured 2σ Doppler spreads between 5 and 30 Hz were observed regularly at night with the lower values corresponding to conditions where the scattering function was dominated by specular-multipath returns or by a single, large feature on the delay-Doppler plane. The specular-multipath condition is most likely to occur when the probing frequency is below the direct path MUF but it may also be observed at frequencies above the direct path MUF, in association with strong off-path irregularities.

During the daytime, for magnetically "quiet" conditions, $K_p < 2$, (K_p is a standard 3 h planetary index of magnetic activity) there is evidence that the transauroral channel behaves like a quiet, mid-latitude channel. During magnetically "unsettled" conditions ($2 \leq K_p \leq 3$), Doppler and delay spreads for the daytime transauroral channel tend to increase somewhat, but they are well below the extreme values that are usually associated with the transauroral channel. Finally, earlier investigators have demonstrated, and the Northern Exposure 92 measurements have confirmed, that "active" magnetic conditions ($3 < K_p < 4$) or "minor magnetic storm" activity ($4 \leq K_p \leq 5$) can initiate a daytime spread F disturbance producing channel characteristics resembling those of the nighttime channel.

Preliminary theoretical calculations by Bello (Wagner et al., 1989) indicate that spread conditions such as those encountered on the nighttime transauroral channel require a signal power margin of up to 14 dB over that of an equivalent additive white Gaussian noise channel for a comparable bit error rate. Given the reduced signal level of the nighttime transauroral scatter signal relative to a reflected signal (−30 dB for the peak signal level and −20 dB for an incoherent Rake output signal, based on Northern Exposure 92 measurements), it would appear that the required signal power margin would be between 14 and 20 dB depending on the Rake's ability to accurately compensate for the channel dispersive effects.

NORTHERN EXPOSURE 92: AN INVESTIGATION OF TRANSAURORAL HF RADIO SKYWAVE PROPAGATION

1. INTRODUCTION

HF skywave communication, by virtue of its exploitation of the Earth's ionosphere for the reflection of radio waves, was the first truly global communication system. The process of radio wave reflection from the ionosphere, however, is not as simple as light reflecting from a highly polished mirror. The ionosphere is a refractive medium whose refractive index depends primarily on frequency and electron density. The mechanism of "reflection" is actually a process of gradual bending of the radiowave rays while transiting the medium. The ionospheric critical frequency is the maximum frequency reflected by the ionosphere at vertical incidence and is determined by the maximum electron density in the medium. All frequencies below the critical frequency are reflected from the bottomside ionosphere regardless of incidence angle on the ionosphere. Radiowaves at frequencies above the critical frequency may be retarded by the ionosphere in propagating at normal incidence but will manage to escape without reflection. The same radiowaves that escape when normally incident on the ionosphere, may be reflected when launched at a sufficiently oblique angle. In all cases of "reflected" signals, the height of reflection and the distance to the ground intercept point* will depend on the frequency, the incidence angle on the ionosphere, and on the shape and critical frequency of the ionosphere.

Because of its dispersive character, the ionosphere introduces delay distortion of transmitted signals. Furthermore, for a given path and ionosphere, the strong dependence of refractive index on frequency establishes a maximum usable frequency (MUF)† for the path. These factors, in combination with the well known time variability of the unperturbed ionosphere, have made the effective use of the HF skywave communication channel, at best, an art that requires the skills of an experienced operator. During periods of ionospheric disturbance, or on channels that are regularly disturbed (e.g., the nighttime auroral channel), even the skills of an experienced operator can be of limited value.

The geostationary satellite radio repeater, operating at much higher frequencies and with proportionately larger bandwidths, has managed to circumvent most of the problems of HF skywave propagation and has displaced the HF skywave link as the primary mode of global communication. Geostationary satellite technology is not without its own problems, however. The enormous expense of building and placing a satellite in proper orbit leads to a highly centralized system subject to catastrophic breakdown. In addition, satellite systems encounter some disruption due to transmission through the

Manuscript approved May 24, 1993.

*For a specific ionospheric shape and critical frequency f_{crit} and for each frequency f such that $f > f_{crit}$, there is a minimum-range ground intercept point, the "skip distance" that increases monotonically with frequency.

†The skip distance for the MUF on a given path is equal to the path length. All frequencies below the MUF have skip distances that are shorter than the path length and hence illuminate the receiver location. For any frequency exceeding the MUF, the receiver terminal lies within the skip zone for that frequency and hence is not illuminated by direct reflection from the ionosphere.

ionosphere under severe disturbance conditions. Finally, the extreme polar regions are not within line of sight of geostationary satellites and therefore cannot use this service.

The advent of spread spectrum communication techniques and the parallel development of VLSI technology have made possible the implementation of wideband HF technologies that promise to mitigate some of the shortcomings imposed by the ionosphere on HF skywave radio systems. In particular, a wideband adaptive HF Rake system (WBHF-Rake), which functions as an adaptive matched filter to the channel, has the ability to equalize the dispersive channel, thereby eliminating the deleterious effects of channel delay dispersion. The degree to which this can be achieved depends on the extent of the dispersive delay spread and on the relative rate of change of the medium compared with the adaptive rate of the Rake (Bello, 1988).

The channel scattering function (Bello, 1963; Stein, 1987) is a concept that arises in the modeling of random scatter channels. It describes the way in which signal energy is redistributed in delay and Doppler as a result of distortion introduced by the transmission channel. Delay spread, a normal result of propagation via the dispersive ionospheric medium, is significantly enhanced by multipath or scatter effects when the medium is irregular and the irregularity structure is spatially extensive. Doppler spread, a consequence of the time variability of the channel, is related to the bulk motion of the irregularity regions and to their turbulent internal motions. Knowledge of the signal-to-noise ratio (SNR) and of spread parameters derivable from the channel scattering function are sufficient for estimating the performance potential of a wideband HF-Rake system on a given channel (Bello, 1988; Wagner et al., 1989).

Channel probe measurements can be used to provide an approximation to the channel scattering function. Measured pulse response functions, each represented by a discrete series of complex valued sample points in the delay variable τ_i and repeated at a series of equally spaced time intervals t_j are Fourier transformed (on the time variable) for each delay value τ_i. The resulting function is analogous to the delay-Doppler spread function defined by Bello (1963). The periodogram represented by the squared magnitude of this function, when smoothed in delay and Doppler, represents an approximation to the channel scattering function. This approximation is used throughout this report and is hereafter referred to as the scattering function. The degree of smoothing used represents a compromise between the conflicting demands of delay and Doppler resolution vs graphical intelligibility.

For acceptance, future generations of HF radio equipment must demonstrate the capability of performing reliably under the most difficult conditions, such as are found in the polar and auroral regions. The primary objective of the Northern Exposure 92 campaign was to explore the performance capabilities of a WBHF-Rake on a skywave channel that is known to be among the most difficult, that is, the transauroral channel. For meaningful results, any communication test must be accompanied by simultaneous measurements of the channel characteristics. In pursuit of that goal, NRL along with the Raytheon Corporation and Mitre Corporation undertook joint measurements on radio links involving transmission via the auroral ionosphere.

A secondary objective of the Northern Exposure 92 campaign was to add to the existing database describing the wideband HF transauroral channel. Published reports on the characteristics of the transauroral channel are not extensive and apply primarily to periods around solar minimum when the mean sunspot number was ~15 (Shepherd and Lomax, 1967; Basler et al., 1987; Wagner et al., 1987 and 1988) and to some near vertical incidence measurements (Wagner et al., 1989; Wagner and Goldstein, 1991), when the mean sunspot number was ~85. The importance of the Northern Exposure 92 measurements lies in the fact that they apply to a time period shortly after the most recent solar maximum. The measurements reported here were made during the period between 13 March and 2 April

1992, which was approximately two years after the peak of the current solar cycle (cycle #22). The mean sunspot number for this period was 108. This compares with a maximum observed sunspot number of 158 for cycle #22 (during June and July, 1989) and a value of 124 during January, 1992, just prior to the measurement period.

This report is devoted to the NRL measurements. Six separate events, spanning a broad range of conditions on the channel, are described. Based on this limited data set, certain general conclusions are drawn regarding the characteristics of the channel. It should be kept in mind, however, that these conclusions are based on a partial study of the Northern Exposure 92 database. Furthermore, it must be borne in mind that the effects of seasonal and solar cycle variations are greatest at high latitudes and that these measurements refer to a specific season (spring equinox) and phase (post solar maximum) of the 11 year solar cycle.

2. BACKGROUND

Conditions in the high-latitude ionosphere are complicated by the diminished role of direct solar radiation in electron density production, and the enhanced role of energetic particle precipitation. Furthermore, magnetospherically controlled plasma convection (Heelis, 1982) has a profound effect on the electron density distribution at high latitudes. Features of the nighttime high-latitude ionosphere that are controlled by the two-cell polar convection pattern include: (1) the formation of the nighttime F layer trough (Knudsen, 1974; Spiro et al., 1978), (2) the transport of very large scale, high-density, solar produced irregularity "patches" from the dayside to the nightside ionosphere (Buchau et al., 1985; Anderson et al., 1987; Knudsen, 1974; Tsunoda, 1988), and (3) the development of relatively thin ($\sim$ 100 km in latitudinal extent), longitudinally extended, high-density, nightside, auroral boundary "blobs" (Robinson et al., 1985). The importance of these large electron density structures (and others related to energetic electron precipitation events) to the formation of nighttime F layer electron density irregularities is considered by Tsunoda (1988) in a comprehensive review article. The conclusion of the Tsunoda review article is that the density gradients inherent in the large-scale irregularities foster a convective instability mechanism that produces a spectrum of field-aligned irregularities ranging in size from $\sim$ 10 km down to $\sim$ 1 m. The same instability processes render the steep electron density gradients at the poleward edge of the nightside F region trough a fertile ground for the production of irregularities. It should be noted that the poleward edge of the nightside F region trough is generally adjacent to the auroral boundary blob region so that both may contribute to irregularity generation at the equatorward edge of the auroral region. Finally, there is substantial evidence (Tsunoda, 1988) for large scale irregularity regions concentrated along the poleward boundary of the auroral region as well as precipitation produced irregularities within the auroral region.

The thrust of the Tsunoda review article is that electron density irregularities are to be found primarily within large-scale electron density enhancement structures called patches and blobs. However, substantial evidence based on satellite in situ measurements (Singh et al., 1985) and HF backscatter measurements (Bates, 1959 and 1960), shows that irregularities are widespread in the auroral ionosphere. Bates' measurements indicate that 5 to 50 m irregularities are a regular and widespread feature of the winter nighttime auroral ionosphere, but are very much weaker, or absent, during the late spring and summer periods of sustained daylight. Furthermore, sunrise and sunset measurements (Bates, 1960) indicate that solar radiation appears to repress the development of new irregularities or accelerate the dissolution of existing irregularities. Energy dissipation in a finitely conducting E layer, that is electrically connected to the F layer along highly conducting magnetic field lines, may be responsible for suppressing the irregularity generation process.

It is well known that effective scatter from field aligned irregularities occurs only at or near normal incidence to the magnetic field lines (Booker, 1956). This implies that HF waves must first be directed at or refracted to normal incidence before they can be effectively scattered by field aligned irregularities. At high latitudes, geomagnetic field lines are nearly vertical, which means that only waves that are in the process of being reflected by the ionosphere can be scattered. But ionospheric refraction decreases with increasing frequency, and higher frequency rays must therefore be launched at shallower angles to achieve normal incidence. Higher frequency rays, launched at shallower angles, must travel longer distances before reflection, consequently they are returned at increasing delays. Echoes received in this manner are called "slant" echoes and they are characterized by a monotonic increase of delay with observing frequency (Bates, 1959). Slant echoes of this type are observed only at high latitudes and it appears that near-vertical geomagnetic field lines are a prerequisite for their occurrence.

In the case of backscatter, each scattered ray retraces its path back to the source regardless of the location of the scatterer, and consequently all rays that manage to achieve perpendicularity with field aligned irregularities contribute to the backscattered echo. Echoes that have the same round trip travel time will add (taking appropriate account of any phase differences). Because of the spatially dispersed scattering medium, echoes will arrive over an extended delay interval defining a time dispersed pulse return from the extended medium. A form of focussing called least-time focussing (Peterson, 1951; Bates, 1959) leads to a substantial enhancement of the leading edge of the weak backscatter return.

In the case of a bistatic geometry, irregularity regions that contribute to the received slant F signal are confined to those locations from which the scattered ray can be refracted to the receiver location. Assuming vertical geomagnetic field lines and a one dimensional ionosphere, those locations are equidistant from the transmit and receive sites. Regions contributing to bistatic slant echoes must, therefore, be located in a narrow vertical slab passing through the path midpoint and oriented perpendicular to the plane of the great circle path (GCP) between transmitter and receiver.* Because of this restriction, one expects that bistatic slant echoes should be weaker than backscatter (monostatic) slant echoes.

A second type of auroral HF backscatter, "strong" scatter, has been observed in the winter, daytime, auroral ionosphere and depends upon partial reflection at the sharp, field aligned boundary of a thin, discrete patch of enhanced electron density (Bates, 1960). Strong scatter derived its name from the fact that its detectability, using early sounder equipment, did not depend on the availability of a "least-time" focussing mechanism. Slant rays and refraction to perpendicularity are involved in strong backscatter, but the localized character of these patches and of the reflection boundary results in scatter echoes that exhibit a nearly constant delay with frequency. For the same reasons, these echoes show much less delay dispersion, at any given frequency, than do the weak scatter echoes.

The weak scatter process involves a Bragg resonant interaction between the probing wavelength and a specific wavelength component of the spectral decomposition of refractive index in the irregular medium. In the case of backscatter, the relevant irregularity scale size is always equal to half the radio wavelength (in the medium). In the case of forward scatter, the wavelength dependence is more complicated and involves the path geometry as well as the radar wavelength. For the simplified model

*This restriction assumes vertically oriented geomagnetic field lines and an ionosphere that is symmetrically distributed about the path midpoint. Recognizing that the geomagnetic field lines are not precisely vertical at the path midpoint and that the ionosphere is not truly symmetrical about the path midpoint, one must expect departures from this simplified model for the revelant scattering region. Nevertheless, it is quite clear that the region that can contribute to the bistatic slant F scatter echo is considerably more restricted than that which contributes to the backscatter slant F echo.

of an assumed planar Earth-ionosphere geometry, the relationship between the irregularity scale length Λ and the probe free space radio-wavelength λ is given by

$$\Lambda = \lambda_r / (2 * \sin(\theta/2))$$

$$\lambda_r = \lambda / \sin(\Phi_0)$$

where θ is the angle between the incident and scattered rays measured at the point of scatter, λ_r is the probe radio-wavelength in the medium at the point of scatter, and Φ_0 is the ray angle of incidence at the bottom of the ionosphere. Taking refraction into account, and assuming vertical magnetic field lines, θ is 0° for bistatic scatter from a point in the vertical (great circle) plane containing the transmitter and receiver, and the irregularity interaction scale length is infinite. As the scatter region is laterally displaced from this plane, θ increases and Φ_0 increases. For very large lateral displacements, θ approaches 180° while Φ_0 approaches 90° and the resonant interaction scale length approaches $\lambda/2$.† In terms of the resonant scatter interaction, this implies that the very largest irregularity scale sizes are responsible for slant echoes scattered from regions nearest the path midpoint and received with near minimum delay. Slant scatter echoes received at increasing delays resonantly interact with progressively smaller scale lengths.

There is a large body of evidence, based upon satellite scintillation measurements, satellite in situ electron density measurements, and radar backscatter measurements, that ionospheric F region electron density irregularities are well described by a power law wavenumber spectrum, with spectral index $p \sim -2$ (Tsunoda, 1985; Singh et al., 1985). A wave number spectrum of this form with a spectral index of -2 implies roughly a 10 dB reduction in wavenumber spectral intensity for each factor of 3 reduction in irregularity scale length. As previously mentioned, a reduced resonant scale length corresponds to an increased echo delay, which implies that the intensity of the slant scatter return from a given irregularity region should decrease exponentially with increasing delay.

It is important to note that an analytical solution of the problem of the propagation of HF radiowaves through an irregular ionosphere is currently available (Nickisch, 1992). The Nickisch approach requires a specification of the background ionosphere for purposes of ray-path determination and uses a multiple thin-screen diffraction model to simulate the effects of the irregular ionosphere. By allowing the diffraction properties and the drift velocity of the medium to vary from screen-to-screen, Nickisch is able to simulate the effects of a nonuniformly irregular medium. Using this technique he has been able to reproduce scattering functions measured by Basler et al. (1987) on a polar path.

3. EXPERIMENT DESCRIPTION

The primary channel under investigation in this experiment was a 1300 km link between Sondrestrom, Greenland (67° N, 50° 43' W) and Keflavik, Iceland (64°N, 22° 36' W). The link geometry is graphically illustrated in Fig. 1. This path was selected because it provides a one hop propagation path of moderate range with a nighttime midpath point that lies within the auroral zone under all conditions of geomagnetic disturbance. During the daytime, the midpath point for the path is subauroral for all conditions except those related to a major magnetic storm. The time interval about local noon for which the midpath point is subauroral gradually decreases, as the level of magnetic disturbance increases from quiet to storm-time conditions. These properties are illustrated in Fig. 2, which shows the position of the path midpoint (a circle at approximately 72° geomagnetic latitude)

†For a lateral displacement equal to the separation of transmitter and receiver, and assuming planar Earth and planar ionosphere geometry, the resonant scale length is calculated to be approximately $1.25 * \lambda$.

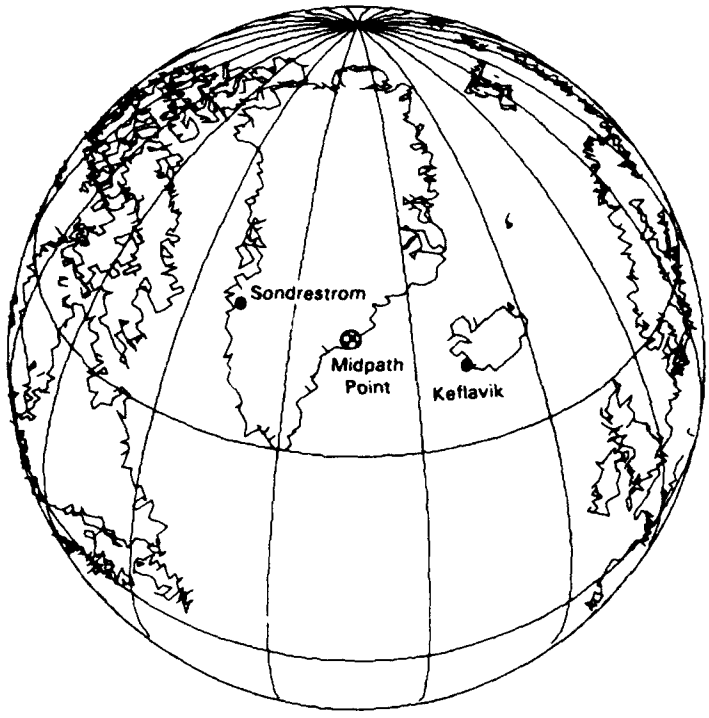

Fig. 1 — Link Geometry, Sondrestrom to Keflavik

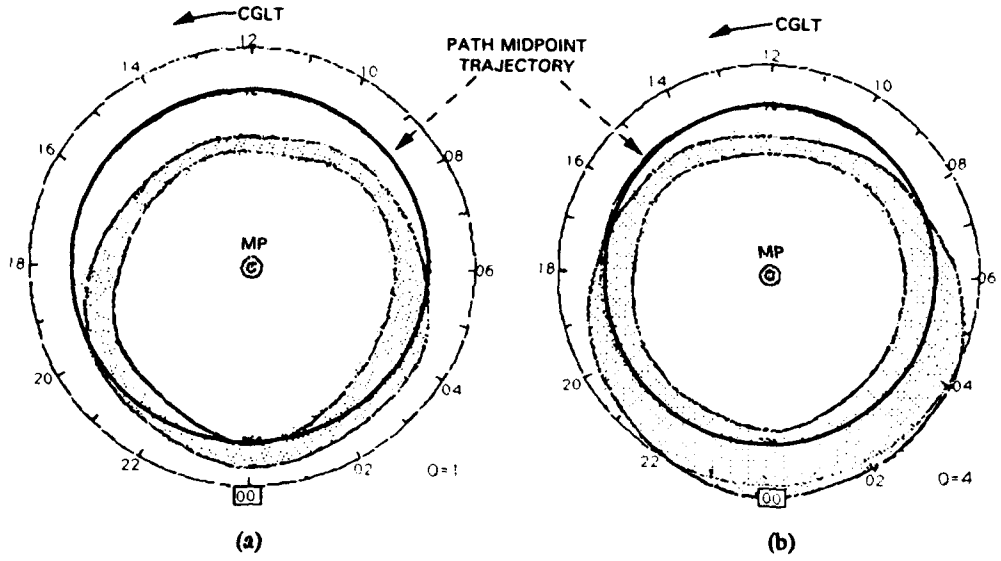

Fig. 2 — Position of path midpoint relative to the auroral oval vs corrected geomagnetic latitude (a) Q = 1; (b) Q = 4

relative to the auroral oval as a function of corrected geomagnetic local time (Whalen, 1970) for two values of the auroral disturbance index Q (Q = 1, Fig. 2(a); Q = 4, Fig. 2(b)).

A wideband HF transmitter, supplied by the Mitre Corporation and located at Sondrestrom, was modified so as to be compatible with the Raytheon Corporation WBHF-Rake receiving equipment situated at Keflavik. The NRL channel probe, operating on the same path and at adjacent frequencies, was used to simultaneously and continuously monitor the channel. A series of observation periods was established, with heavy emphasis on the late evening to early morning hours, when the most difficult propagation conditions were expected. Measurements were made primarily when the conditions appeared to be most challenging for HF propagation. Operating frequencies were selected on the same basis.

In addition to the wideband Rake communication system and the HF channel probe, ionospheric conditions on the path were also monitored by using a BR Communications Corp. chirpsounder. The chirpsounder transmitter was provided by Mitre and was located at Sondrestrom. The chirpsounder receiver was provided by NRL* and colocated at Keflavik with the Raytheon WBHF-Rake receiver system and the NRL HF channel probe receiver. All systems at a given site either shared antennas or used separate but identical antennas.

Measurement periods were organized into time blocks of varying length (between 4 and 8 h). Control of the HF transmitter was shared between the Sondrestrom-Keflavik path and a secondary path between Sondrestrom and Bedford, Massachusets. The second path was manned exclusively by Mitre personnel using the Mitre wideband HF Rake and its associated channel monitoring system.

A frequency for the WBHF-Rake was selected from a list of authorized frequencies on the basis of channel conditions as revealed by the chirpsounder. NRL would then select probe frequencies adjacent to that of the WBHF-Rake but sufficiently distant so as not to significantly raise its noise floor. The channel probe and the HFWB-Rake would then run simultaneously for a period of approximately 25 min. During this time the channel probe would collect data on channel conditions while the HFWB-Rake would log its operating status, monitor its communication performance, and periodically check the condition of the channel on its frequency. Spot probing of the channel by the WBHF-Rake system on its frequency served as a useful check on the relevance of the NRL channel probe measurements to the WBHF-Rake channel.

Most of the channel probe measurements used two probe frequencies, offset by ± 400 kHz from the WBHF-Rake frequency. Occasionally, a slightly larger or smaller offset was required because of the presence of strong interferers at the standard offset. On a few occasions, when propagation conditions or other factors prevented the use of two bracketing frequencies, only one probe frequency was used.

Magnetic conditions from 1 January 1991 and through the measurement period (13 March to 2 April 1992) are represented in Figs. 3(a) and 3(b) by the daily planetary magnetic index, Ap. Figure 3(a) indicates very active magnetic conditions, including several major magnetic storms, in the roughly 425 days prior to the start of the measurement period. Magnetic conditions during the Northern Exposure measurement period were substantially calmer, with magnetic activity varying between "quiet" and "active." This is evident from Fig. 3(b), which is an expanded view of the latter part of Fig. 3(a), which covers the measurement period.

Altogether, NRL conducted a total of 97 separate experiments for a total observation time of approximately 37 h. Of these, 72 experiments were conducted with two probing frequencies,

*The chirpsounder receiver is on loan to NRL from the Voice of America (VOA).

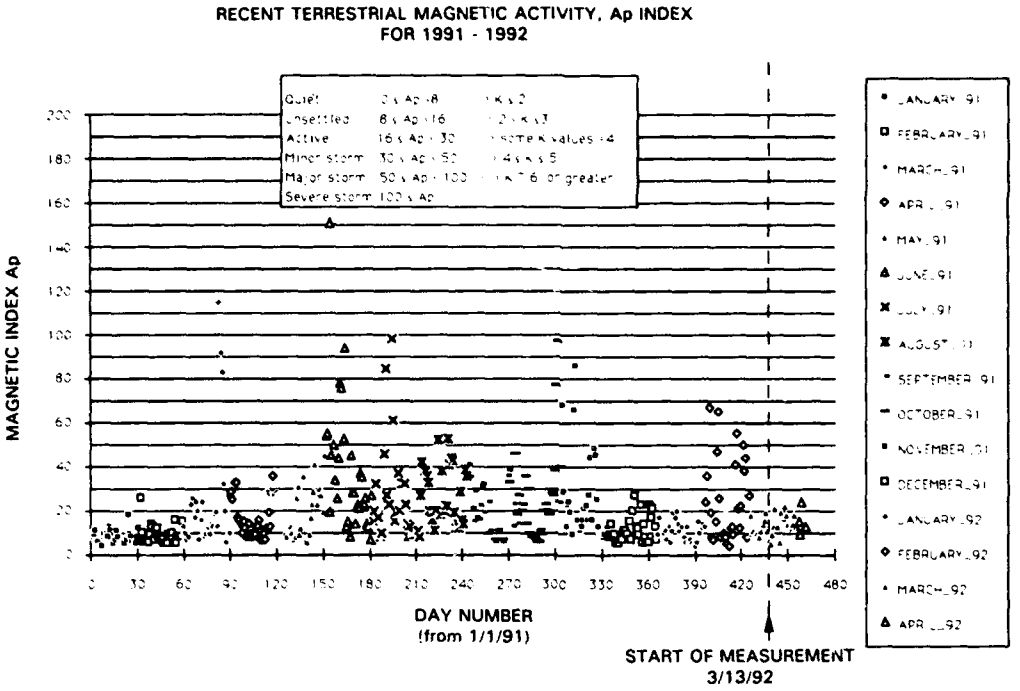

Fig. 3(a) — Recent geomagnetic activity, 1 Jan 1991 to 4 Apr 1992

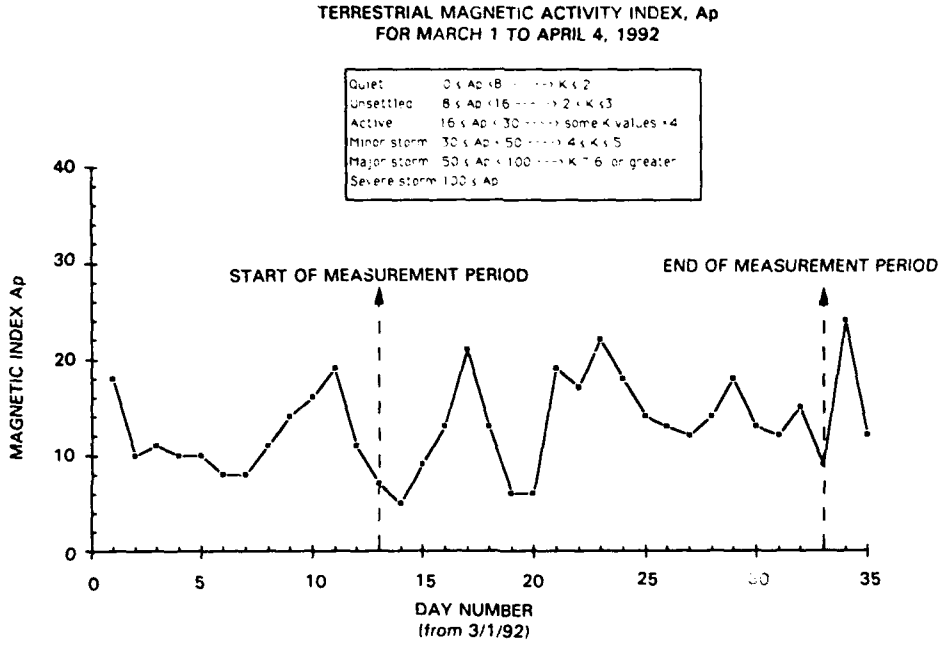

Fig. 3(b) — Geomagnetic activity during the Northern Exposure measurement period

3 experiments involved only one frequency, and an additional 22 experiments were multifrequency measurements involving 5 or 6 frequencies that usually covered a range of 5 to 6 MHz. The multifrequency measurements were designed to provide a broader picture of channel conditions than could be obtained at only two frequencies. Multifrequency channel probe operations were usually conducted at times when the Sondrestrom-Bedford path controlled the wideband HF communications transmitter and were therefore not accompanied by Raytheon WBHF-Rake operation. Figure 4 provides a graphic illustration of measurement periods superimposed on a calendar with dates represented by rows and time of day by columns. Time is presented as universal time (UT) and is subdivided into 3-h intervals as is commonplace in presentations of geomagnetic activity data. Shaded areas represent measurement periods. The number printed in each 3-h date-time cell indicates the reported planetary magnetic index K_p for that period.

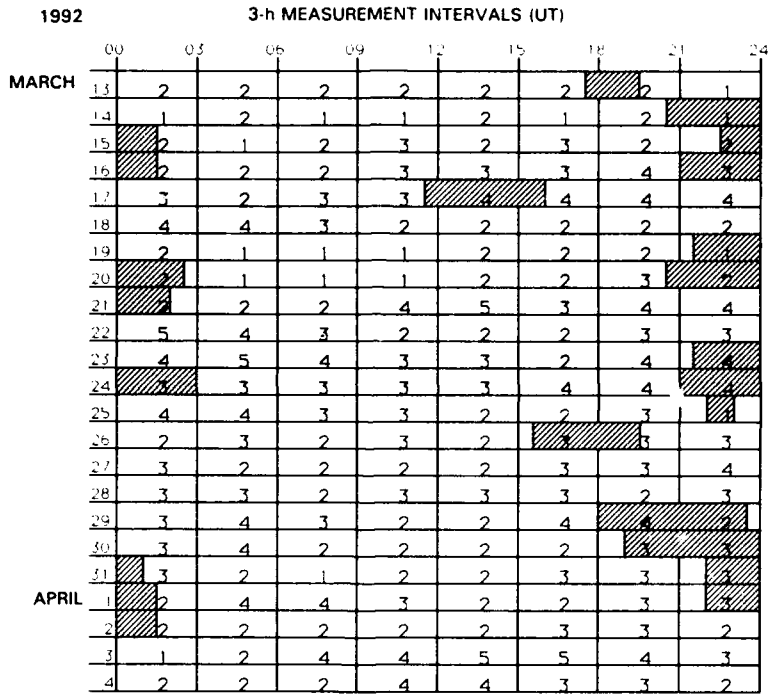

Fig. 4 — Calendar of recorded 3-h planetary magnetic index K_p and probe observation periods

During these measurements, primary interest was placed on propagation via the one hop F2 layer mode. During unsettled or active magnetic conditions, reflections from an underlying sporadic-E layer would frequently block ("blanket") reflection from the ionospheric F layer. This frequently frustrated efforts to monitor what otherwise promised to be excellent observing conditions. During these times, control of the communications transmitter was passed to the Sondrestrom-Bedford link, which was usually unhindered by sporadic E blanketing of the F layer return. On a few occasions, communication was attempted via the sporadic E layer with interesting results.

A table listing all channel probe experiments performed during the Northern Exposure 92 exercises is contained in the appendix. The table lists the date, experiment start time, PN sequence chip length, number of frequencies probed, delay resolution, effective pulse width of the probe signal, and the width of the Doppler window supported by the measurement. A quick glance through the table will show that most of the experiments required the maximum width Doppler window, in keeping with the objective

of seeking measurements pertaining to the most difficult channel conditions. Daytime measurements were generally not expected to exhibit large Doppler shifts or spreads. For these cases, an experiment format that provided enhanced delay resolution at the expense of Doppler window width (sampling rate) was prepared. During actual measurements, however, we encountered very few cases where the narrower Doppler window (± 2.2 Hz) was adequate to the needs of the measurement.

Our operations in Greenland were subject to the condition that they be conducted in a manner that would not interfere with air traffic control activities based in Sondrestrom. This limited operations at frequencies below 11 MHz, which essentially excluded operations during early morning hours when the MUF for the Sondrestrom-Keflavik path descended below 10 MHz.

Auroral absorption, a potential obstacle to measurement operations and communications in the auroral region, was never a factor. Although most measurements were made under magnetic conditions for which absorption would not be expected, some measurements were made during periods of sustained magnetic activity, of magnitude $K_p = 4$, with no evidence of enhanced absorption. Other auroral zone measurements, made under similar magnetic conditions but with the D layer pierce points approximately 3° further south than those for this path, were subject to radio blackout for a considerable period of time surrounding the peak of a $K_p = 4$ magnetic disturbance (Wagner et al., 1991). This suggests that the magnetic latitude of the Sondrestrom-Keflavik path is sufficiently high that propagation is unaffected by auroral absorption.

4. NRL CHANNEL PROBE DESCRIPTION

The NRL Channel Probe is a wideband, bistatic, time domain channel probe developed at NRL for the purpose of investigating the wideband properties of the HF radio channel. The probe measures the complex pulse response of the radio channel at a number of different frequencies in the HF band. It operates at signal bandwidths of 31.25 kHz, 125 kHz, 250 kHz, and 1 MHz with effective prober pulse widths of 32 μs, 8 μs, 4 μs, and 1 μs, respectively. The transmitter and receiver are programmed to step through the frequency band in synchronism according to a preprogrammed table of frequencies. Repeated measurements at a given frequency are necessary for observing the fast fluctuations of the received signal. The sampling interval of repeated pulse response measurements is variable and supports unambiguous Doppler windows ranging between ± 0.8 Hz and ± 2.2 Hz in our standard operating format, and between ± 7.7 Hz and ± 30.6 Hz in our extended Doppler format.

The transmitter uses a spectrum spreading coded modulation that is processed at the receiver in a fast, real-time correlation processor to produce the effect of a short-pulse sounding signal. The coded modulation signal is a continuously repeated, maximal length, pseudonoise (PN) binary sequence that bi-phase modulates the transmitted carrier. Two PN sequences are available, one of 255 chips and a second of 2047 chips, supporting narrowband and wideband operation, respectively. The duration of the 255 chip sequence is 8.16 ms corresponding to a chip rate and system bandwidth of 31.25 kHz. The duration of the 2047 chip sequence is 8.188 ms corresponding to a chip rate and system bandwidth of 250 kHz. A 25% duty factor pulse modulation, superimposed on the bi-phase modulated carrier, can be used to expand the basic system bandwidths of 31.25 kHz and 250 kHz to 125 kHz and 1 MHz, respectively.

Figure 5 shows a block diagram of the channel probe instrument . Time synchronism and phase coherence between transmitter and receiver are assured by the presence of very stable and accurate frequency and time sources at both sites. The frequency standard at the transmitter site is a cesium beam reference oscillator, while the one at the receiver site is a rubidium vapor resonance oscillator. Clock

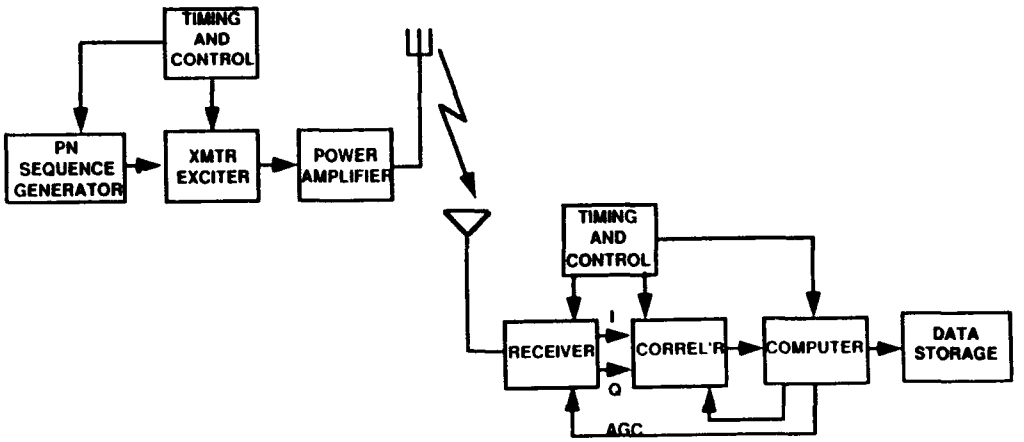

Fig. 5 — Channel probe block diagram

synchronization is established at transmitter and receiver sites to a relative time accuracy of better than 10 μs using either LORAN C, GPS broadcast time, or a combination of the two.

The transmitter signal consists of a phase stable reference at a frequency of 39.5 MHz, which is bi-phase modulated by the PN sequence. Depending on the bandwidth requirements of the measurement, the signal may also be pulse modulated by a 25% duty factor pulse modulation for a 4:1 bandwidth expansion. The signal is then amplified, down-converted to the desired HF frequency, amplified and filtered at HF, and delivered to the transmitting antenna. All oscillators are locked to the station frequency standard.

The radio receiver is a phase stable heterodyne receiver with computer controlled intermediate frequency ($i - f$) amplifier gain and local oscillators locked to the station frequency standard. The output of the i - f amplifier is converted to in-phase and quadrature-phase baseband video components that are filtered, amplified, sampled at the sequence chip rate, and converted to a 12 bit digital representation of the received signal(s). The digitized signals are then passed to a real-time correlator unit for cross correlation with a series of delayed replicas of the transmitted PN sequence, thereby producing a sampled representation of the channel pulse response. The sampled, pulse response output of the correlator is then passed to the system computer for further screening and for recording on disk and then to magnetic tape for permanent storage.

The start of a measurement, specified to a resolution of one minute, is precisely controlled by an automatic "clockstart" at each site. Thereafter, experiment synchronization is maintained by using extremely accurate clock pulse generators to "strobe" Control Microprocessors at the two locations. Frequency and other experiment parameters are controlled by the microprocessors that have been preloaded with identical parameter sets and frequency tables.

For a case involving no amplitude modulation, the autocorrelation function of the PN sequence consists of a triangular peak of height equal to the number of chips, N, in the sequence and a base that is twice the chip width. The triangular peak rises above a uniform pedestal of amplitude -1. The amplitude of the pedestal relative to the correlation peak is N^{-1} leading to a pedestal that is ideally 48 or 66 dB below the peak, depending on whether one is using a 255 or a 2047 chip sequence. For cases involving pulse modulation of the sequence with a 25% duty factor, the width of the main peak is reduced by a factor of four while the height of the peak is unchanged. In addition,the uniform pedestal is replaced by a series of triangular peaks of amplitude -1, of width equal to that of the main peak, and separated

in delay by the chip width. These are the so-called time sidelobes of the correlated sequence. The pedestal and the time sidelobes are frequently visible when using the 255 chip sequence in a low-noise environment. Evidence of this feature has never been seen when using the 2047 chip sequence.

Channel probe operation is very flexible since the operating format is software or firmware controlled. Standard operating procedure usually consists of an initial narrowband "sounder" run that makes a single pass, in relatively fine frequency steps, through the range of frequencies supported by the ionosphere. The purpose of this run is to collect data for a premeasurement ionogram and also to locate those delay intervals occupied by the various propagating ionospheric modes. The sounder mode is followed by an extended period of probing (prober mode) that can be narrowband (255 chip) or wideband (2047 chip). After probing is completed, a second sounder run is executed that produces a postmeasurement ionogram. Comparison of the before and after ionograms provides a general indication of ionospheric changes incurred over the measurement period.

During standard prober mode operations, repeated pulse response measurements are made on a limited set of frequencies of interest. The sequence in which measurements are made is determined by the scientific objectives of the experiment. In cases where interest is in the relatively slow ionospheric changes associated with the passage of acoustic gravity waves or traveling ionospheric disturbances (TID's), a round robin format is used in which a single pulse response measurement is made on each frequency in turn. This is known as our sequential-scan format. In cases where one is interested in more rapid fluctuations, it is necessary to dwell at each frequency while making repeated pulse response measurements, before proceeding to the next frequency in the table. This operational format is dubbed our dwell-scan mode and the maximum sampling rate currently achievable in this mode is 4.4 Hz.

In a number of interesting cases, such as those where the ionosphere is characterized by a condition known as spread F, the signal fluctuation rate can exceed the maximum sampling rate afforded by dwell-scan operation. In these cases, the extended Doppler format is used. By sacrificing delay resolution for improved time resolution, the extended Doppler format permits sampling rates of approximately 61.2 Hz (Doppler window of ± 30.6 Hz).

5. RESULTS

The Northern Exposure 92 measurement database is quite extensive. It consists of 97 experiments comprising approximately 5000 MBytes of pulse response data. This summary report presents a representative sampling of the data for a variety of channel conditions and experimental formats. In this section, examples of channel data, ranging from relatively benign to what would be generally accepted as very difficult conditions, are presented. General ionospheric conditions are summarized by timely oblique ionograms for the bistatic path while channel conditions are succinctly described by scattering functions that illustrate the dispersion of signal energy in delay and Doppler engendered by its passage through the channel.

Important signal and channel characteristics are evaluated for each case considered and are summarized in Table 1. Parameters included in Table 1 are: (1) mean signal delay, (2) delay spread, (3) mean Doppler shift, (4) Doppler spread, (5) channel spread factor, (6) peak signal spectral amplitude, (7) total signal energy, and where applicable, (8) average spectral noise level, and (9) the ratio of peak spectral amplitude to average spectral noise. Signal amplitude is represented in decibels relative to an arbitrary reference level. System output noise is represented in the same way so as to provide a meaningful reference for the signal amplitude representation. Delay spread and Doppler spread are represented by twice the standard deviation of the spread about their respective means (the 2σ spread).

Table 1 — Measured Channel

Experiment No.	Date	Time (UT)	Frequency (MHz)	K_p Index	Mean Delay (ms)	2σ Delay Spread (μs)	Mean Doppler (Hz)	2σ Doppler Spread (Hz)	Spread Factor	Spectral Peak (dB)	Integrated Power (dB)	Avg Noise (dB)	Spectral Peak to Avg Noise (dB)
—	—	—	—	—	—	—	—	—	—	—	—	—	—
2	3/13/92	18:06:28	18.6	2	4.97	50	0.9	1.7	8.50E-05	78.5	97.6	NA	NA
2	3/13/92	18:07:27	19.4	2	5.129	166	−0.3	1.8	2.99E-04	70.2	95.8	NA	NA
4	3/13/92	19:13:40	18.6	2	5.125	223	−3.9	1.4	3.12E-04	82.8	98.3	25.4	57.4
4	3/13/92	19:01:51	19.4	2	5.162	212	−4.6	1.2	2.54E-04	72.1	88.9	30.9	41.2
10	3/14/92	22:42:31	13.5	1	5.88	376	−2.3	6	2.26E-03	50.1	74.7	21.9	28.2
20	3/15/92	0:04:02	8.8	2	5.441	607	−4.2	8.4	5.10E-03	79.3	102.4	47.3	32
42	3/19/42	23:10:59	16.6	1	7.759	892	−1	21.8	1.94E-02	41.6	69.2	15.8	25.8
42	3/19/92	23:13:25	15.8	1	7.421	668	−1.9	26	1.74E-02	45.1	73.3	30.2	14.9
43	3/19/92	23:38:22	16.6	1	7.251	1141	4.2	20.7	2.36E-02	41.6	72.4	21.5	20.1
43	3/19/92	23:39:29	16.6	1	7.184	1087	12.9	20.4	2.22E-02	41.8	73.3	22.4	19.4
43	3/19/92	23:43:47	15.8	1	6.923	822	16.5	16.9	1.39E-02	45.7	73.6	25.5	20.2
43	3/19/92	23:44:09	15.8	1	6.924	702	15.7	14.1	9.90E-03	47.9	76.6	37.2	10.7

Channel spread factor is represented as the dimensionless product of the 2σ delay spread and the 2σ Doppler spread.

Other comments relating to general atmospheric conditions and speculation as to the character of the reflecting medium are included in each case. For all but one of the cases, results are presented in the form of a "snapshot" of conditions on the channel. One case of special interest, i.e., the one exhibiting the largest spread factor based on a preliminary perusal of the data, is considered in greater detail. For that case, curves are presented showing the variation of all important channel variables over the 25 min time span of the measurement.

Times of all events are represented in terms of UT, which is the local time used in Iceland. Magnetic local time (MLT), which is the time scale most meaningful for describing auroral phenomena, is approximately UT -1 h at the midpath point of the Sondrestrom-Keflavik path.

CASE 1: March 13, 1992; Start Time = 17:57 UT; Exp #2
Probe Frequencies of 18.6 and 19.4 MHz
$K_p = 2$

At this time of day and season, the sun is approximately 24° above the horizon as viewed from a height of 200 km above the path midpoint. Direct photon effects are declining but we are still dealing with a daytime ionosphere, albeit one in which the F2 layer predominates over the F1 layer. For a K_p value of 2, the path midpoint lies slightly equatorward of the auroral oval, and the path segment between Sondrestrom and the path midpoint lies partially within the auroral oval as indicated by reference to plastic overlays of the auroral oval upon the northern polar region (provided by N. Gerson).* Furthermore, the Gerson overlays indicate that the measurements were made approximately 2 h before the intrusion of the nighttime F layer trough on the path.

The conditions experienced on this path, as indicated by the ionogram of Fig. 6(a) (made at 17:50 UT with a BR Communications chirpsounder), could be characterized as mildly unsettled based on the absence of clearly defined ordinary (O) and extraordinary (X) mode traces near the MUF ($\sim$20 MHz). The ionogram shows some indication of weak scatter at frequencies just above the MUF, which is not uncommon and is evidence of weak irregularity structure in the medium. Prior NRL measurements that were made at Fairbanks, Alaska at roughly the same local magnetic time but for quiet magnetic conditions ($K_p \leq 1$, unpublished data), were characterized by propagation conditions comparable to those on a quiescent, daytime, mid-latitude path. The differences between these and the Alaska measurements may be attributed to the fact that the midpath point of the Sondrestrom-Keflavik path lies approximately 5° further north (geomagnetically) than the Fairbanks path, and that these measurements were made during unsettled magnetic conditions, i.e., $K_p = 2$.

The chirpsounder ionogram (Fig. 6(a)) is presented in a conventional two-dimensional (2-D) ionogram format, with the shaded curve above the ionogram indicating the measured SNR vs frequency. The ionogram presents data over a 5 ms delay interval but is not calibrated in terms of absolute delay. An equivalent ionogram (Fig. 6(b)), made at approximately 17:57 UT from channel probe measurements, presents essentially the same information as that of Fig. 6(a) but in a somewhat different format. The probe ionogram presents a 3-D ionogram over a 3.2 or 5 ms delay interval and

*The Gerson overlays are a convenient representation of the "Feldstein ovals" (Feldstein and Starkov, 1967) over a map of the northern polar region in corrected geomagnetic coordinates, after Whalen (1970). The Feldstein ovals are a set of representations of the auroral oval in corrected geomagnetic latitude and corrected geomagnetic local time based on measurements of the visible aurora over a wide range of disturbance conditions.

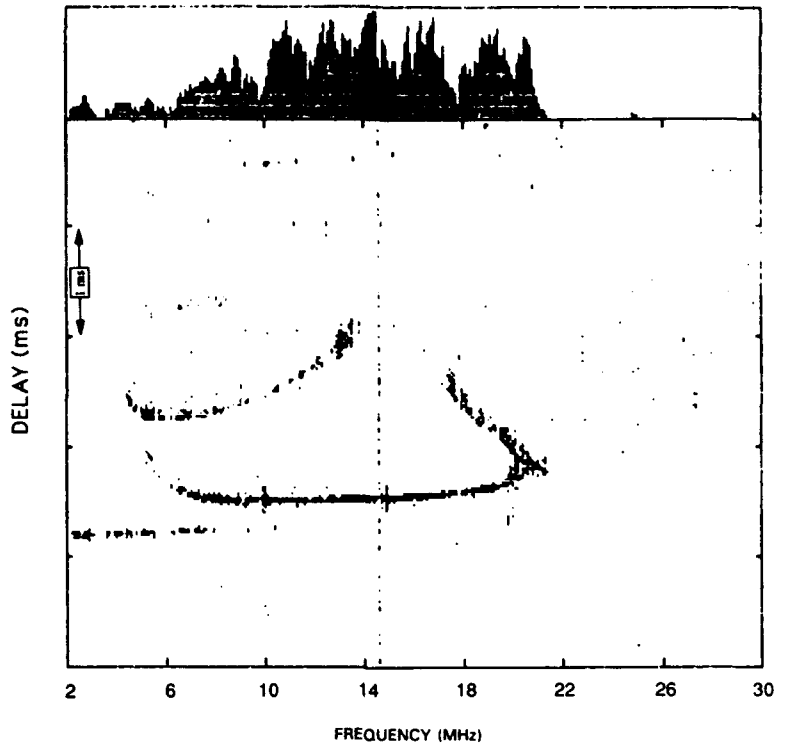

Fig. 6(a) — Chirpsounder ionogram, Sondrestrom to Keflavik, 13 March 1992, 17:50 UT

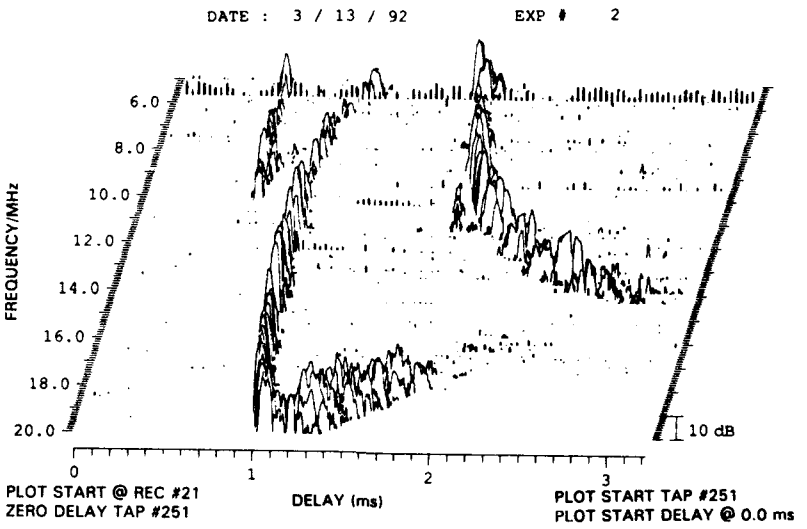

Fig. 6(b) — Probe ionogram, Sondrestrom to Keflavik, 17:57 UT (origin of delay scale = 4.0 ms)

measured delay is accurate to ~10 μs. The actual delay corresponding to the delay axis origin can vary from one ionogram to another, and its value is indicated in the figure caption. In Fig. 6(b), the delay origin is 4.0 ms. Later data sets will use one or the other of these two ionogram formats depending on which is more informative in a given case.

Because it was anticipated that relatively modest Doppler spreads would be encountered during this measurement, a dwell-scan format affording a Doppler window of $\pm$2.18 Hz was used. The 2047 chip sequence (no pulse modulation) was selected for the measurement in order to provide a delay resolution of 4 μs. Because of the large number of pulse response samples generated by the 2047 chip sequence (most of which are noise), amplitude thresholding and delay windowing of the data are required for the computer to cope with the data thruput. Amplitude thresholding is designed to discriminate against noise returns in favor of signal returns. An undesirable consequence of amplitude thresholding is that it makes it impossible to accurately estimate the average noise level.

Frequencies of 18.6 and 19.4 MHz were used in this experiment because they were situated close to the MUF and, judging from the appearance of the ionograms (Figs. 6(a) and 6(b)), offered the best chance of exhibiting multipath propagation. Figure 7 shows two views of a scattering function for the F2 layer, low-ray return at 18.6 MHz, one from head-on and above (Fig. 7(a)), and the other from the right side and above (Fig. 7(b)). The scattering function is shown relative to a plot floor located approximately 24 dB below the spectral peak. Figure 7 shows evidence of a main return commencing at a delay of 12 μs on the plot and of additional returns of lesser power and exhibiting substantially different Doppler shifts.

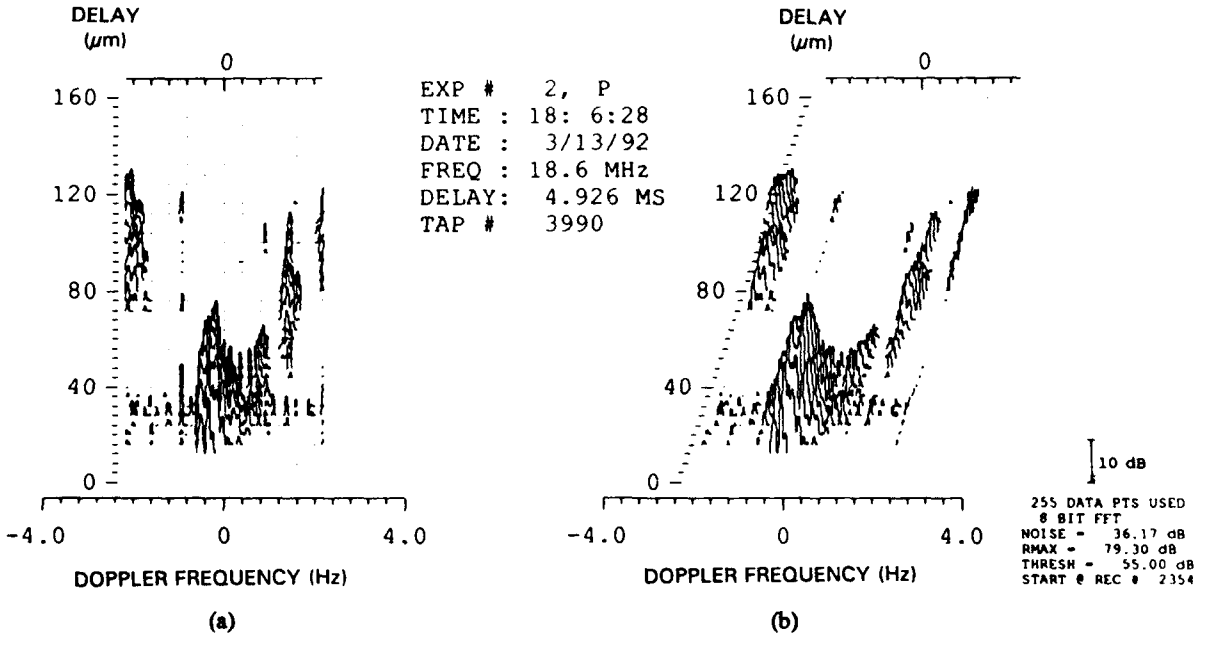

Fig. 7 — Scatter function, 1F2 low-ray return, late afternoon conditions, K_p = 2, 18.6 MHz, (a) 3-D head-on view, (b) 3-D oblique-angle view (origin of delay scale = 4.926 ms)

The main return, which appears to be made up of more than one multipath component, is characterized by a mean Doppler shift of -0.26 Hz and a 2σ spread about the mean of 0.31 Hz. The observed minimum delay of approximately 4.94 ms corresponds to a virtual height of reflection of approximately 350 km, which is not unreasonable for a frequency near the MUF on this path and at this time of day. Assuming that the reflection point is near the path midpoint, the observed Doppler shift is most likely the result of an increasing layer height for the late afternoon ionosphere.

The signal return appearing at -2 Hz and 80 μs in Fig. 7 must be caused by reflection from an "off-path" irregularity region. It is obviously aliassed, leading to some uncertainty as to whether it represents a signal with a negative Doppler shift that extends slightly beyond the negative limit of the Doppler window, or a signal with a positive Doppler shift that extends well past the positive limit of the window. Lowering of the plot floor reveals the presence of additional low level spectral structure appearing at predominantly positive values of Doppler shift. The irregularity region responsible for the low level returns is assumed to also be responsible for the aliassed return and a positive Doppler shift is therefore assigned to it. Taking account of all multipath components, and assigning a positive Doppler shift to the aliassed component, the calculated values of mean Doppler shift and 2σ Doppler spread work out to be 0.9 and 1.7 Hz, respectively.

Measurements were also made at a second frequency (19.4 MHz) during experiment #2. This frequency was closer to the MUF for the path with the result that the high and low rays form an almost continuous return in the signal delay variable. The scattering function shown in Fig. 8 shows an expanded view (0 to -2 Hz) of the dominant component at 19.4 MHz, and shows two views, Figs. 8(a) and 8(b), corresponding to the two views of the scattering function displayed in Fig. 7. The positive half of the Doppler spectrum (not shown here) contains additional reflected returns whose Doppler shifts and delays correspond to those of the secondary features of Fig. 7 and are presumed to be caused by reflection from the same off-path irregularity region(s). This observation provides additional support to the assertion of a positive Doppler shift for the aliassed component at 18.6 MHz.

The multipath character of the main return in Fig. 8 is evident from its complicated structure. The scattering function indicates two major features at different delays but covering roughly equivalent ranges of Doppler. These represent the low ray (early return) and the high ray (late return) corresponding to the two possible propagation paths for point-to-point skywave propagation. Both components are observed to consist of several multipath components, which is indicative of a mildly irregular ionosphere. For these results to be considered in a proper perspective, it should be pointed out that the scattering function for a comparable mid-latitude path, at the same time, season, and phase of the solar cycle, would show four distinct ridge-like structures rather than the confused assortment of returns as are present in Fig. 8. These would correspond to low-ray O and X modes, and high-ray O and X modes. The mean Doppler shift and Doppler spread for the main return at 19.4 MHz are -0.7 and 0.52 Hz, respectively, which compares with values of -0.26 and 0.31 Hz for the corresponding quantities at 18.6 MHz.

The plot floor in Fig. 8 is arranged to be higher (20 dB below the peak spectral amplitude) than is required for the suppression of noise clutter on the plot. The reason for selecting the higher plot floor is to emphasize the dominant spectral components of the signal return. Lowering the plot floor to 30 dB below the peak spectral amplitude reveals the presence of additional low level scatter returns that fill the Doppler window but are confined to a 300 μs delay interval. The Doppler window width is clearly inadequate for accurately defining the Doppler spread of the low-level scatter returns. One must therefore conclude that even under relatively quiet magnetic conditions, scattered

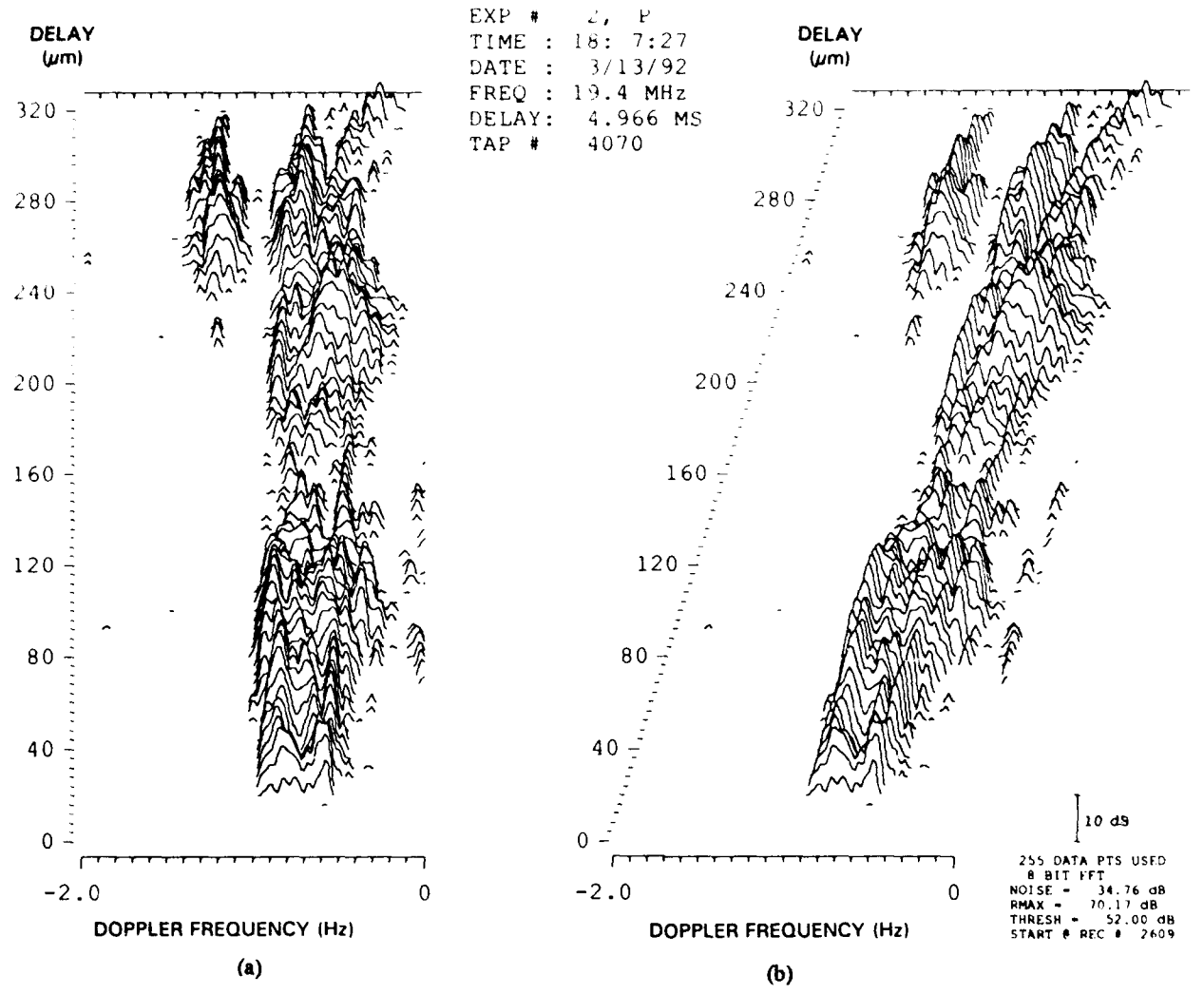

Fig. 8 — Scatter function, 1F2 return, late afternoon conditions, K_p = 2, 19.4 MHz, (a) 3-D head-on view, (b) 3-D oblique-angle view (origin of delay scale = 4.966 ms)

returns can occupy a Doppler range in excess of 4.4 Hz. Ignoring any aliassing of low-level returns at 19.4 MHz, but otherwise taking account of all Doppler components, the mean Doppler shift and 2σ Doppler spread are computed to be −0.34 Hz and 1.8 Hz, respectively.

Parameters summarizing characteristics of the received signals at 18.6 and 19.4 MHz are presented in Table 1.

CASE 2: March 13, 1992; Start Time = 1900 UT; Exp #4
Probe Frequencies of 18.6 and 19.4 MHz
K_p = 2

Experiment #4 followed experiment #2 by approximately 1 h. Because of its characteristic shape, which is thicker on the nightside than on the dayside, the equatorward edge of the auroral oval appears to have moved to a lower magnetic latitude at the magnetic meridian of the path midpoint at this time. This causes more of the path between Sondrestrom and the path midpoint to

be included within the auroral oval. The F layer trough, on the other hand, is not yet a factor on the path segment between Keflavik and the path midpoint. In anticipation of more disturbed propagation conditions, the experiment format was modified to accomodate an unambiguous Doppler window of ± 7.66 Hz. In order to accomodate the higher pulse response sampling rate required by the wider Doppler window, the delay sampling rate had to be decreased. The resulting delay resolution of the measurement was 32 μs.

Frequencies of 18.6 and 19.4 MHz were used as probing frequencies in experiment #4, as was the case in experiment #2. The probe ionogram (Fig. 9) shows what appear to be strong multipath returns from approximately 18 MHz up to the maximum sounding frequency of 20 MHz. Figure 10, (a) and (b), shows the scattering function for the return at 18.6 MHz. The figure on the right (b) is a 3-D representation of the scattering function similar to the figure on the right in Figs. 7 and 8. The figure on the left (a) is a 2-D contour plot describing the energy distribution of the scattering function by a series of intensity contours on the delay-Doppler plane. The contours represent energy levels in decibels relative to the peak energy of the scattering function. Their values are shown in the box labelled contours. The individual contours are not labelled on the plot but their values should be apparent from the context. The format of Fig. 10 will be followed in all subsequent scattering function diagrams that are presented.

The energy of the scattering function in Fig. 10 is confined to the negative half of the Doppler plane except for a weak spurious return at positive Doppler frequencies that should be ignored.* The scattering function appears to consist of a main low-ray return plus a weaker high-ray return at a greater delay. In addition, the contour plot of the scattering function indicates a widespread distribution of scattered signal energy at the -20 to -30 dB level filling the entire range of delays between low and high rays, and extending over a Doppler range of ~ 4 Hz.† If one considers the 2σ values of the spread parameters, however, one obtains considerably more modest values of spread, which emphasizes the dominance of reflected or strongly scattered signals over weakly scattered signals. The calculated values of Doppler shift and 2σ Doppler and delay spreads for the 18.6 MHz signal are -3.9Hz, $+1.4$ Hz, and 223 μs, respectively.

Figure 11, (a) and (b), shows the scattering function for 19.4 MHz. There is clear evidence of a low ray and of its delay extension that encompasses a weaker high ray. The -20 to -30 dB contours (Fig. 11(a)) are fairly broad as was the case at 18.4 MHz. The 2σ value of Doppler spread is again much more modest than that indicated by the -30 dB contour. Calculated values of Doppler shift and 2σ Doppler and delay spread are -4.6 Hz, $+1.2$ Hz, and 212 μs, respectively.

Results for experiment #4 indicate large differences in Doppler shift from those characterizing experiment #2. The rate of ionospheric rise required to produce a Doppler shift of -5 Hz at these frequencies and for this path is approximately 80 m/s, which is a rather large rate of rise. It is possible, however, that gravity waves moving through the ionosphere could introduce large changes of Doppler shift over the time period in question. Examination of the complete Doppler time history for experiments 2, 3, and 4 would be required to make a more definitive statement regarding the nature and causes of the observed Doppler shift.

Summary parameters for the return signals at 18.6 and 19.4 MHz are included in Table 1.

*The spurious return is a reduced (~ -25 dB) mirror image of the real return and is associated with small departures from 90° phase difference between the quadrature components of the receiver baseband video.

†Scatter returns can be seen down to a level of -40 dB but this does not significantly alter the shape of the scattering function diagram of Fig. 10. The -40 dB contour encompases a Doppler spread of ~ 5 Hz and a delay spread of ~ 1 ms.

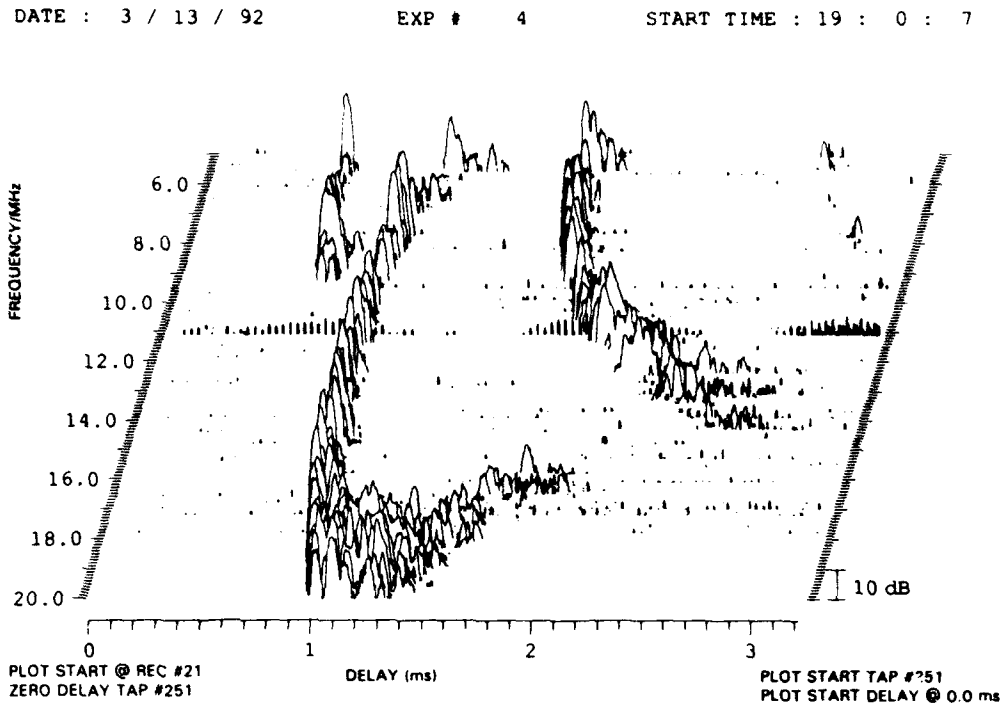

Fig. 9 — Probe ionogram, Sondrestrom to Keflavik, 19:00 UT, (origin of delay scale = 4.0 ms)

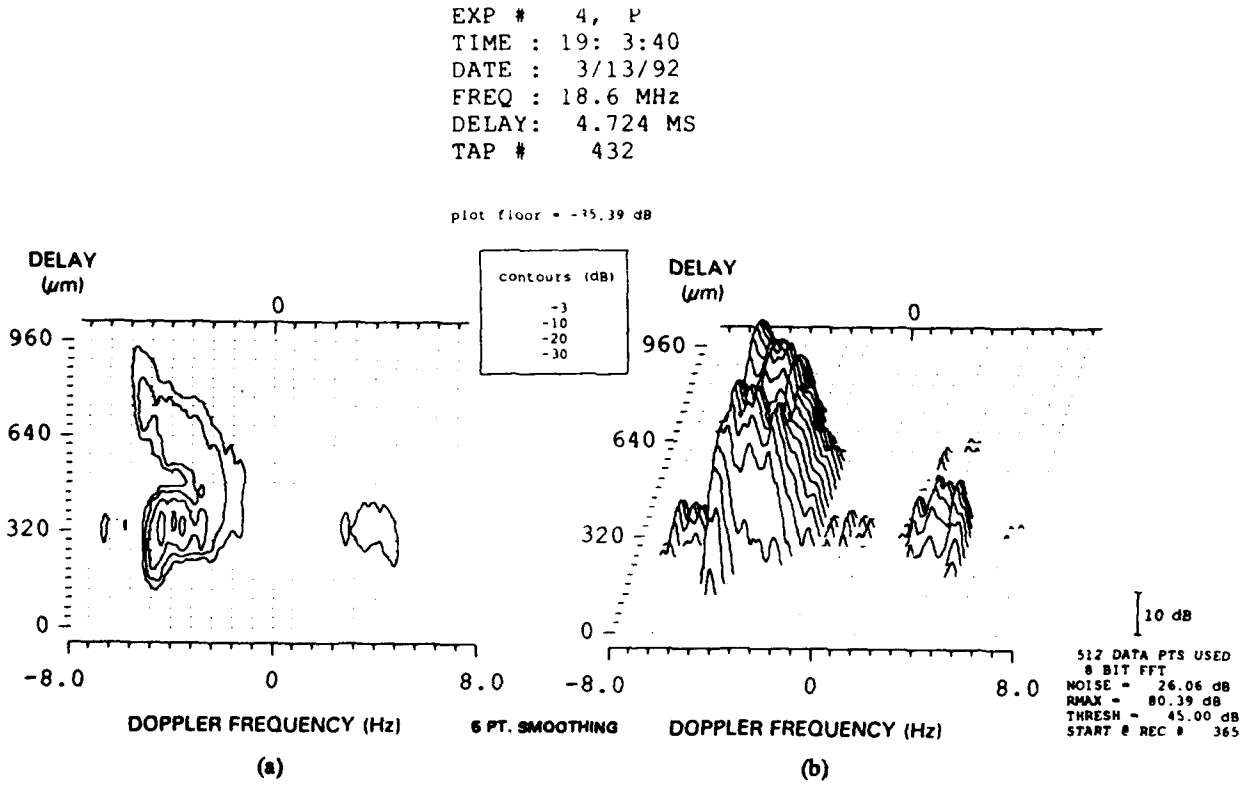

Fig. 10 — Scatter function, 1F2 return, late afternoon conditions, K_p = 2, 18.6 MHz, (a) contour plot, (b) 3-D oblique-angle view (origin of delay scale = 4.724 ms)

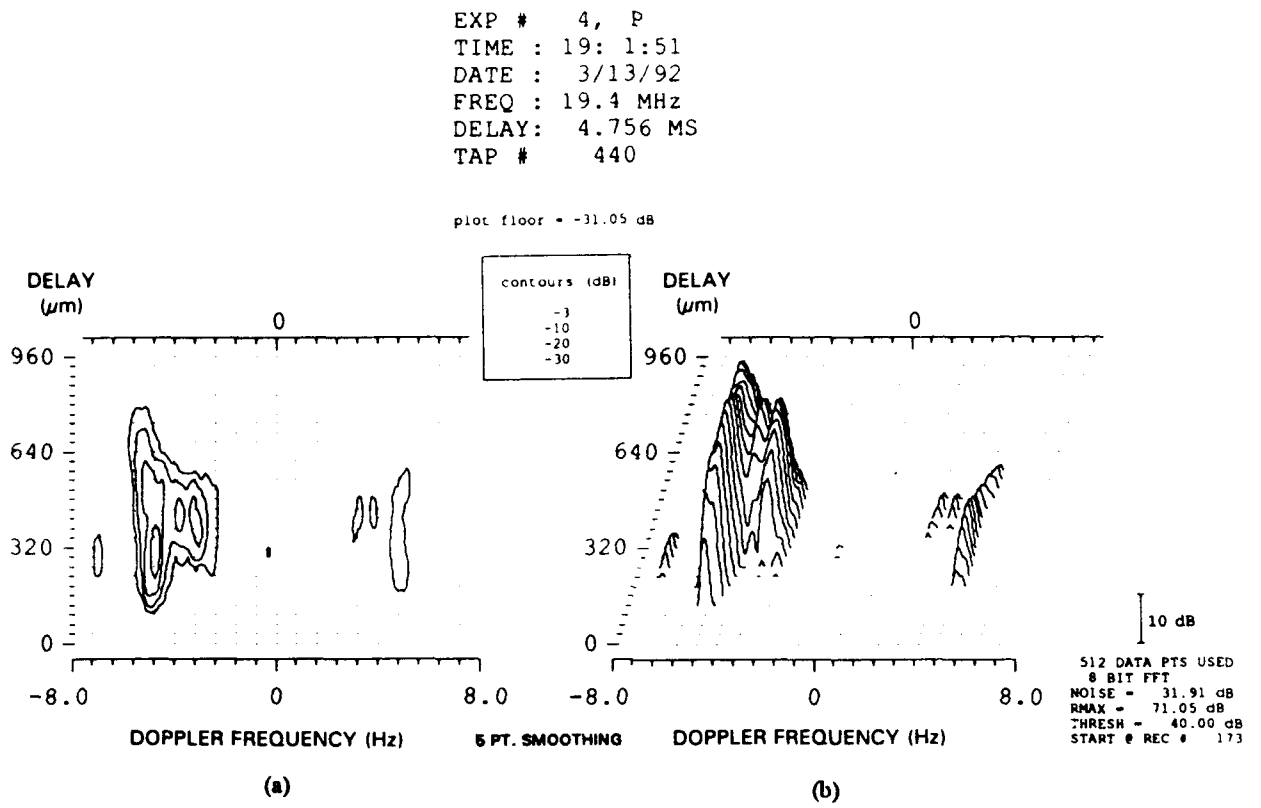

Fig. 11 — Scatter function, 1F2 return, late afternoon conditions, K_p = 2, 19.4 MHz, (a) contour plot, (b) 3-D oblique-angle view (origin of delay scale = 4.756 ms)

CASE 3: March 14, 1992; Start Time = 22:39 UT; Exp #10
Probe Frequencies of 13.5 and 14.3 MHz
K_p = 1

Experiment #10 was conducted during the premidnight period of the nighttime auroral oval. Reference to the Gerson overlays indicates that the midpath point lies within the relatively narrowly defined auroral oval. In addition, the path between midpath and Keflavik traverses the nightside F layer trough region, which may extend the region of auroral irregularities equatorward of the auroral oval. A chirpsounder ionogram made approximately 5 min before the probe measurement (Fig. 12) is quite informative as to the state of the ionosphere at this time.* The ionogram indicates the presence of a strong, nonblanketing sporadic E layer plus several diffuse F layer traces. In addition, the ionogram indicates the presence of weak slant F scatter returns at frequencies above 14 MHz.

The least delayed F layer trace is assumed to be associated with an overhead layer. The MUF for this layer is approximately 13 MHz. All other F layer traces are assumed to be oblique path returns from large-scale clouds of enhanced electron density in the vicinity of the great circle propagation path. The diffuse character of all of the traces is an indication of the irregular structure of the corresponding regions. Finally, the presence of weak slant F scatter echoes above the MUF, characterized by a linear increase of minimum delay with increasing frequency, is indicative of a

*A probe ionogram was not available for experiment #10 because of a small timing error between the probe transmitter and receiver. Although adversely affecting the ionogram part of the data acquisition, the timing error had negligible effect on the probe segment of the measurements.

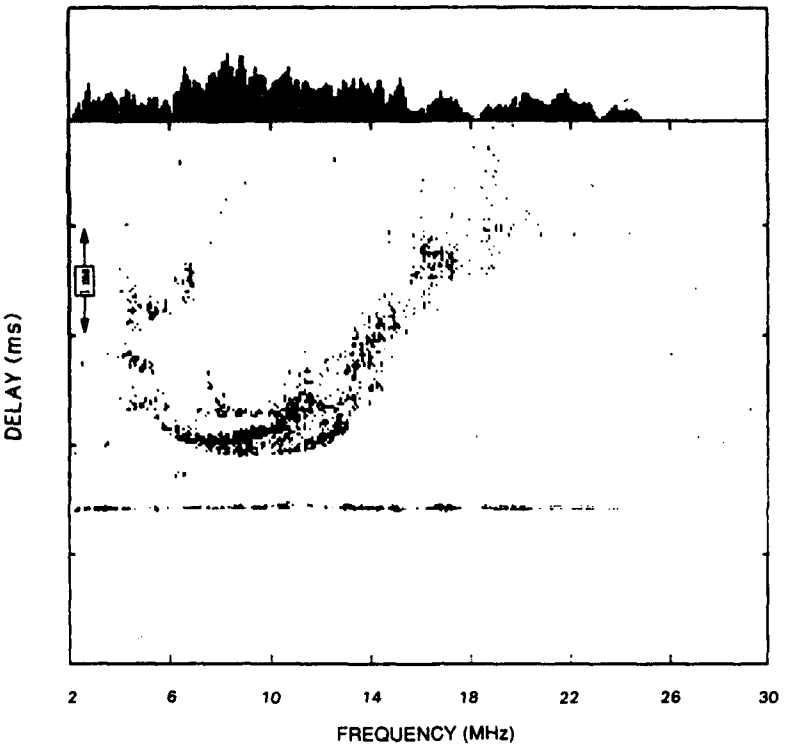

Fig. 12 — Chirpsounder ionogram, Sondrestrom to Keflavik, 14 March 1992, 22:35 UT

nonuniform, but spatially extensive distribution of field aligned irregularities embedded within the ionospheric medium.

Two frequencies were probed during this experiment, one slightly above the MUF at 13.5 MHz and another at 14.3 MHz. Preliminary screening of the data indicated that signals were strong at 13.5 MHz but were too weak to be observed at 14.3 MHz. The data considered here are limited to a single scattering function snapshot at 13.5 MHz (Fig. 13, (a) and (b)). Future analysis should include a more exhaustive search of the entire 14.3 MHz data record. This is warranted because of the observed variability of scatter signals above the MUF.

The scattering function shown in Fig. 13 was formed from pulse response measurements sampled at a maximum rate of 15.32 Hz. This sampling rate supports an unambiguous Doppler window of ± 7.66 Hz. The peak spectral amplitude in the scattering function for 13.5 MHz is between 20 and 30 dB below that of the preceding examples, thus implying that a signal scatter or weak diffraction mechanism predominates over specular reflection in the received signal. Judging from the scattering function shown in Fig. 13, the Doppler window appears to be inadequate to accommodate the Doppler spread of the low-level scatter returns without some aliassing. Clearly, a wider Doppler window would have been desirable for the conditions encountered during this experiment.

Generally speaking, one expects that a logarithmic representation of scattering function amplitude should decrease smoothly with increasing delay, as discussed in Section 2. Spectral features departing from such behavior must be associated with the presence of spatially localized

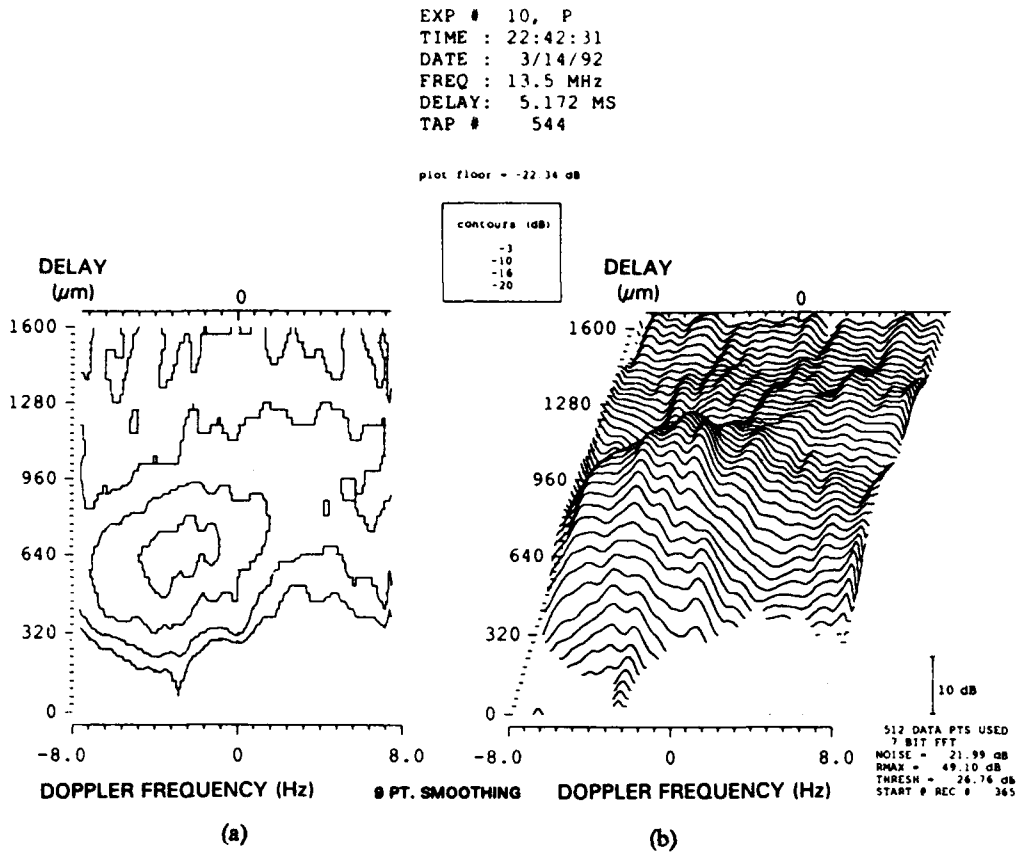

Fig. 13 — Scatter function, 1F2 return, premidnight conditions, K_p = 1, 13.5 MHz, (a) contour plot (b) 3-D oblique-angle view (origin of delay scale = 5.172 ms)

blobs within a general background of weaker field aligned irregularities. Figure 13(b) shows evidence of two such regions. The dominant feature is located at a relative delay of 640 μs and a Doppler shift of ~ -3 Hz. A less prominent feature is located at about the same delay but at a Doppler shift of $\sim +8$ Hz (assuming no aliassing). Each of these returns is undoubtedly associated with one of the delayed traces on the ionogram of Fig. 12. Assuming that the less prominent return is unaliassed (and this is purely conjecture), the Doppler shifts indicate that the stronger return is associated with an irregularity region that is receding from the plane of the GCP while the weaker return is associated with a region that is approaching the GCP.

It is generally true that the 2σ Doppler spread is controlled by the most intense feature (or features) of a signal and that the lower level returns exert a lesser (but not negligible) influence on the computed value of the 2σ Doppler spread. The predominance of the spectral feature at -3 Hz results in a 2σ Doppler spread that is substantially smaller than that occupied by the -20 dB contour of Fig. 13(a). The 2σ Doppler spread, although frequently much smaller than the range of Dopplers occupied by the low level scatter returns, is probably a better indicator of the potential performance of a Rake system than that corresponding to any specific Doppler spread contour. It should be emphasized, however, that the true spread of the lower level returns is not accurately represented by the scattering function of Fig. 13 and that this will introduce an error into the calculation of the 2σ Doppler spread parameter.

A calculation of the channel parameters for the scattering function of Fig. 13, assuming negligible aliassing, reveals a mean Doppler shift of −2.27 Hz and a 2σ Doppler spread of 6 Hz. A tabulation of all relevant channel parameters based on this calculation is included in Table 1.

CASE 4: March 16, 1992; Start Time = 00:01 UT; Exp #20
Probe Frequencies of 8.8 and 9.6 MHz
$K_p = 2$

Experiment #20 was conducted shortly after midnight during unsettled magnetic conditions. The location of the propagation path in relation to the F layer trough and the auroral oval differs from that of experiment #10 because of the later time at which the measurement was made and the larger value of K_p. In this case, the entire half-path between midpath and Keflavik is within the auroral oval, while the path segment between Sondrestrom and the midpath point is essentially within the polar region. The ionogram for this experiment (Fig. 14) indicates a strong one hop F layer trace with extensive range-spread (spread F) at all frequencies. Because of the spread character of the ionogram, it is not possible to define a conventional MUF for the path. Careful examination of the ionogram, however, indicates the presence of what appear to be specular-multipath returns below 11 MHz. The existence of the specular returns would seem to indicate that, were it not for the irregularities, it would be possible to define a MUF whose value would be on the order of 11 MHz.

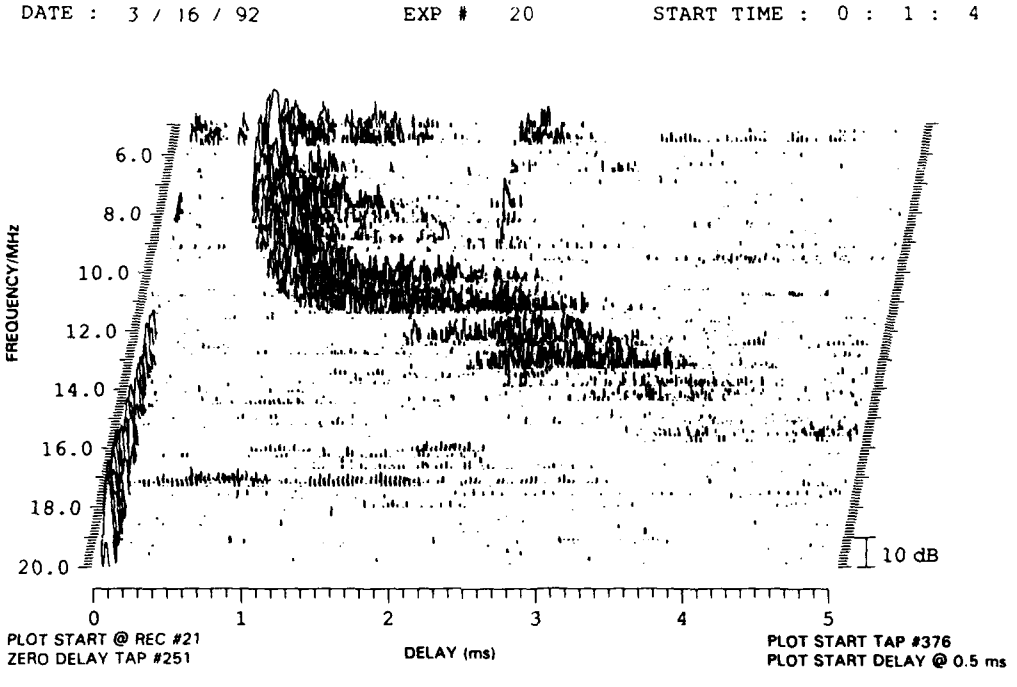

Fig. 14 — Probe ionogram, Sondrestrom to Keflavik, 00:01 UT (origin of delay scale = 4.5 ms)

In addition to the main F layer trace, there is a weak trace delayed by approximately 1.7 ms relative to the main F layer trace. This second trace is apparently associated with off-path reflection or scatter from a distant irregularity region. Finally there is weak evidence of slant F scatter at frequencies above 12 MHz. The evidence for the slant F return is weakened by signal dropouts in several crucial frequency bands and by possible confusion with the second trace at frequencies where the two returns intersect. It is possible that the second trace is an example of the strong scatter

return discussed by Bates, which he observed to merge with the slant F return at its upper frequency limit (Bates, 1960).

The two frequencies selected for probing, 8.8 and 9.6 MHz, were both below the apparent MUF for this path. Of these two frequencies, good signals were observed at 8.8 MHz but no signals were observed at 9.6 MHz. A 2-D ionogram (not shown here) equivalent to that in Fig. 14 reveals a signal gap between 9 and 10 MHz. The absence of signals in this frequency range is most likely caused by a dense "other-user" environment (9.5 to 9.9 MHz is an authorized broadcast band). This explanation is supported by an examination of the receiver $i - f$ amplifier gain, which is AGC controlled, and which indicates a gain differential of -16 dB between 9.6 and 8.8 MHz.

The background noise and interference level at 8.8 MHz is also high (see Table 1). This is not surprising considering that broadcasters tend to move from higher to lower frequencies at night causing congestion in the available spectrum and frequently leading to spillover from assigned bands. An unfortunate consequence of the enhanced noise level is that it limits our ability to detect the weakest scatter signals and to assess the range of Dopplers spanned by those signals.

Figure 15, (a) and (b), shows a snapshot of a scattering function that was taken during this experiment. In this case, as in most other cases (see appendix), a sampling rate of 61.27 Hz was used corresponding to a Doppler window of ± 30.64 Hz. The elevated noise level at 8.8 MHz limits the visibility of scatter returns to within 32 dB of the spectral peak. In spite of this limitation, the scattering function indicates extensive delay and Doppler spread. These large spreads are not reflected in the 2σ values of these parameters, however, because of a localized region of very strong returns that, as in the case of experiment #10, dominate the return. The measured values of Doppler shift and Doppler spread for this case are -4.2 and 8.4 Hz, respectively. These and all of the other scattering function parameters for this experiment are presented in Table 1.

It should be noted that the strength of the spectral peak observed in Fig. 15 is comparable to that received by reflection during experiments 2 and 4 (see Table 1). Furthermore, the measured signal delay is compatible with reflection from or near the path midpoint and, finally, the Doppler width of the spectral peak, as observed on the unsmoothed scattering function (not shown here), suggests Doppler broadening associated with the limited "lifetime" of a reflecting facet. Based on these considerations, it is presumed that the broad peak in the scattering function is the result of specular-multipath or "glint" from large, intense, short-lived reflectors concentrated about the path midpoint. The weaker returns are presumed to be associated with slant F volume scatter from many weaker, smaller-sized, spatially dispersed irregularities. Additional support for the hypothesis of short-lived multipath reflection or glint, can be found on the ionogram of Fig. 14, which contains evidence of very strong individual returns (specular reflections) amid weaker scatter returns at 8.8 MHz.

A second peak in the scattering function of Fig. 15 (~ -10 dB smaller than the main component) can be seen at a relative delay value of 1824 μs. It is part of the delayed trace discussed earlier in this section, and it displays the same limited lifetime spectral characteristics as the main return.

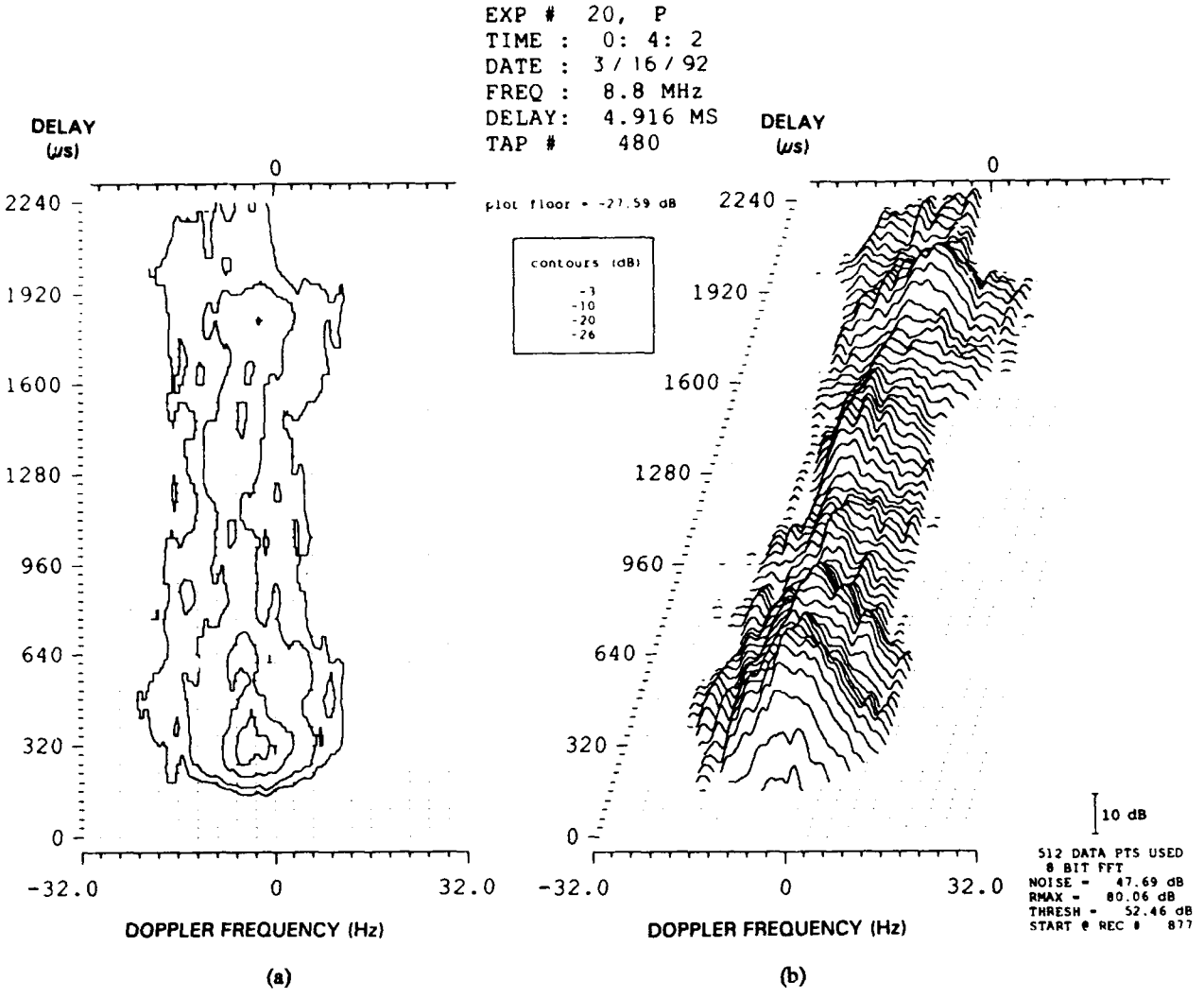

Fig. 15 — Scatter function, 1F2 return, midnight conditions, K_p = 2, 8.8 MHz, (a) contour plot, (b) 3-D oblique-angle view (origin of delay scale = 4.916 ms)

CASE 5: March 19, 1992; Start Time = 23:10 UT;Exp #42
Probe Frequencies of 16.6 and 15.8 MHz
K_p = 1

Experiment #42 was conducted shortly before midnight at a time of relatively quiet magnetic conditions The path midpoint was centered in the auroral oval with the oval occupying approximately the middle third of the path.The segment of the path from Keflavik to the auroral oval was located in the region of the F layer trough while that from the auroral oval to Sondrestrom lay within the polar region. The ionograms for this experiment are shown in Fig. 16(a) (chirpsounder ionogram, 23:20 UT) and Fig. 16(b) (probe ionogram; 23:10 UT; delay origin = 4.5 ms). Both ionograms show evidence of extensive spread F at all frequencies and a rapidly increasing minimum delay vs frequency at the higher frequencies, which is characteristic of slant F scatter echoes from the auroral region. Similar weak, delayed echoes are also visible on the ionograms for experiments 10 and 20 (Figs. 12 and 14), and for experiment 43 (next section, Fig. 19), and appear to be a regular phenomenon during the premidnight and postmidnight hours.

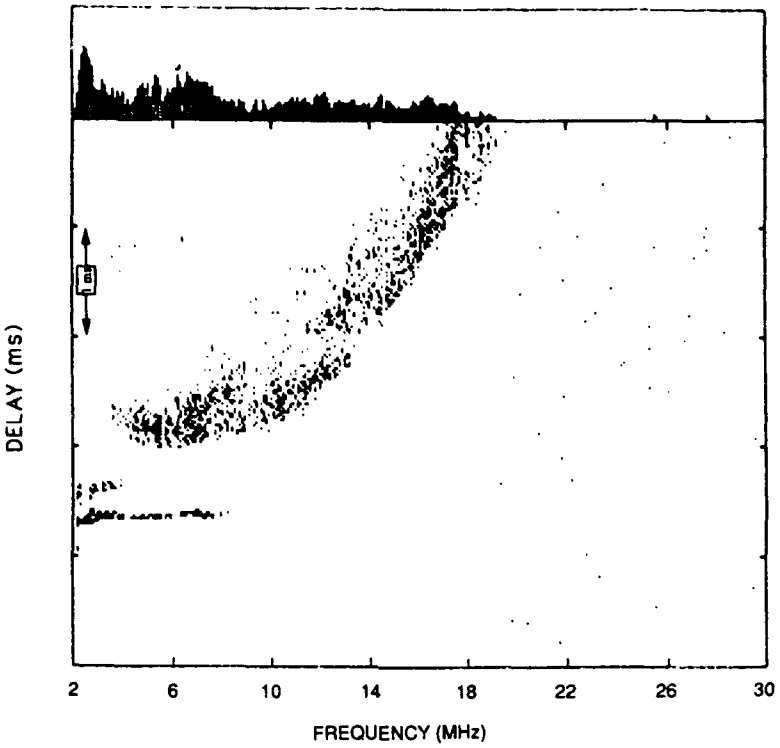

Fig. 16(a) — Chirpsounder ionogram, Sondrestrom to Keflavik, March 19, 1992, 23:20 UT

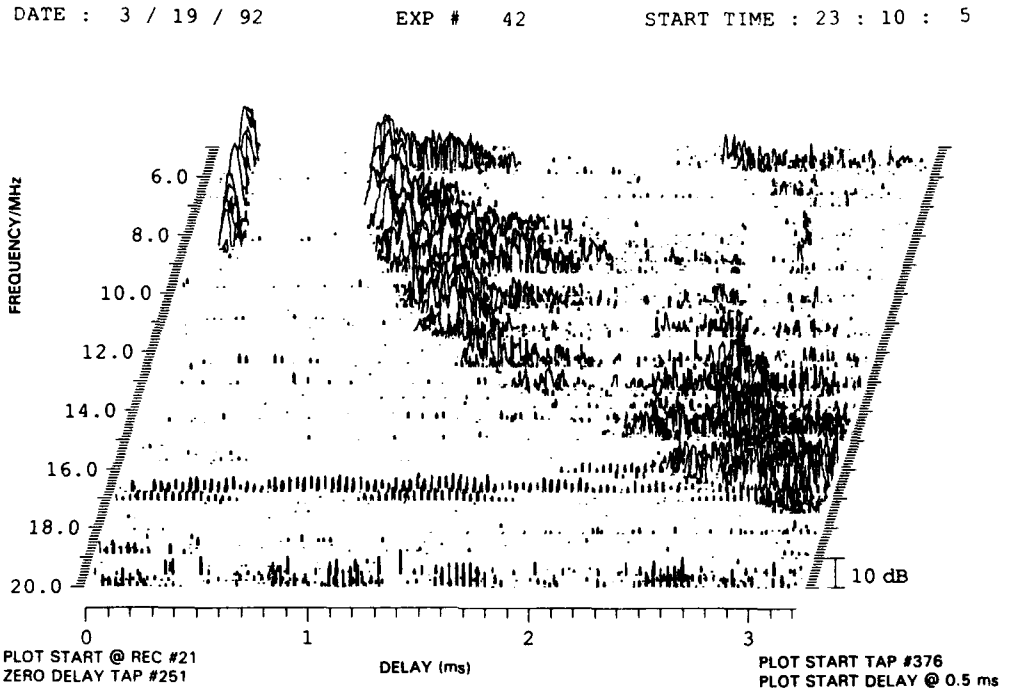

Fig. 16(b) — Probe ionogram, Sondrestrom to Keflavik, 23:10 UT (origin of delay scale = 4.5 ms)

Given that the mechanism for scattering at frequencies above the MUF (when a MUF can be defined) involves scatter from field aligned irregularities, it seems likely that range-spread scatter echoes (spread F*) observed below the MUF are also due to scatter from field aligned irregularities. The extensive delay associated with the range-spread echoes may, therefore, also be attributable to the slant echo mechanism.

Probe frequencies for this experiment were chosen to be sufficiently high to assure a purely slant F scatter channel. A snapshot of the scattering function for a frequency of 16.6 MHz is shown in Fig. 17, (a) and (b). It appears to be dominated by two major components, one at a small negative Doppler shift (~ -8 Hz) and another at a small positive Doppler shift ($\sim +8$ Hz). The peak spectral amplitude observed in this scattering function is ~ 25 to 30 dB smaller than the specular returns observed in experiments 2, 4, and 20, thereby firmly establishing it as a scattered signal. In addition to those two major components, there is a general dispersion of lower level scatter that appears to overflow the Doppler window at a level of approximately -20 dB relative to the spectral peak, but which is confined within the bounds of the Doppler window at a level of -16 dB. In delay, the scatter returns seem to be limited to an interval between 6.9 and 9.3 ms. The calculated values for mean Doppler shift and 2σ Doppler spread are -1.3 and 20.8 Hz, respectively. Values for these and all other calculated channel parameters are listed in Table 1.

At this time of day, the convective motions of the relevant regions of the F layer are sufficiently complex that they probably cannot be characterized in terms of a simple drift motion. Nevertheless, the observed scattering function could be characterized as being dominated by slant returns from two separate high-density patches or blobs, one approaching and the other receding from the plane of the GCP between the transmitter and receiver.

A scattering function for 15.8 MHz (Fig. 18, (a) and (b)), made approximately 2.5 min after the 16.6 MHz measurement, also reveals what appear to be two distinct scattering regions. The 15.8 MHz scattering function appears to be more confined than that at 16.6 MHz, however this is deceptive and is a consequence of an elevated noise and interference background at 15.8 MHz. The higher noise and interference level is confirmed by comparing the measured spectral noise levels (printed in the lower right hand corner of Figs. 17 and 18) and by the recorded i-f amplifier gains during the two measurements. It is interesting to note that the peak spectral level for signal at 15.8 MHz actually exceeds that at 16.6 MHz by about 3.5 dB while its signal-to-noise ratio (SNR) is approximately 11 dB smaller.

Calculated values of Doppler shift and 2σ Doppler spread have been determined to be -1.1 and 27.1 Hz, respectively, and are tabulated in Table 1 along with all other calculated channel parameters. It is interesting to note that the Doppler spread at 15.8 MHz exceeds that at 16.6 MHz despite appearances to the contrary. This is attributable to the relatively uniform spread of energy associated with the scattering function at 15.8 MHz as compared with that at 16.6 MHz. This can be confirmed by examining the contour plots of Figs. 17 and 18 at the -10 dB level.

*All cases of spread F shown in this report fall under the classification range spread. Indeed this appears to be the most common form of spread F observed at high latitudes.

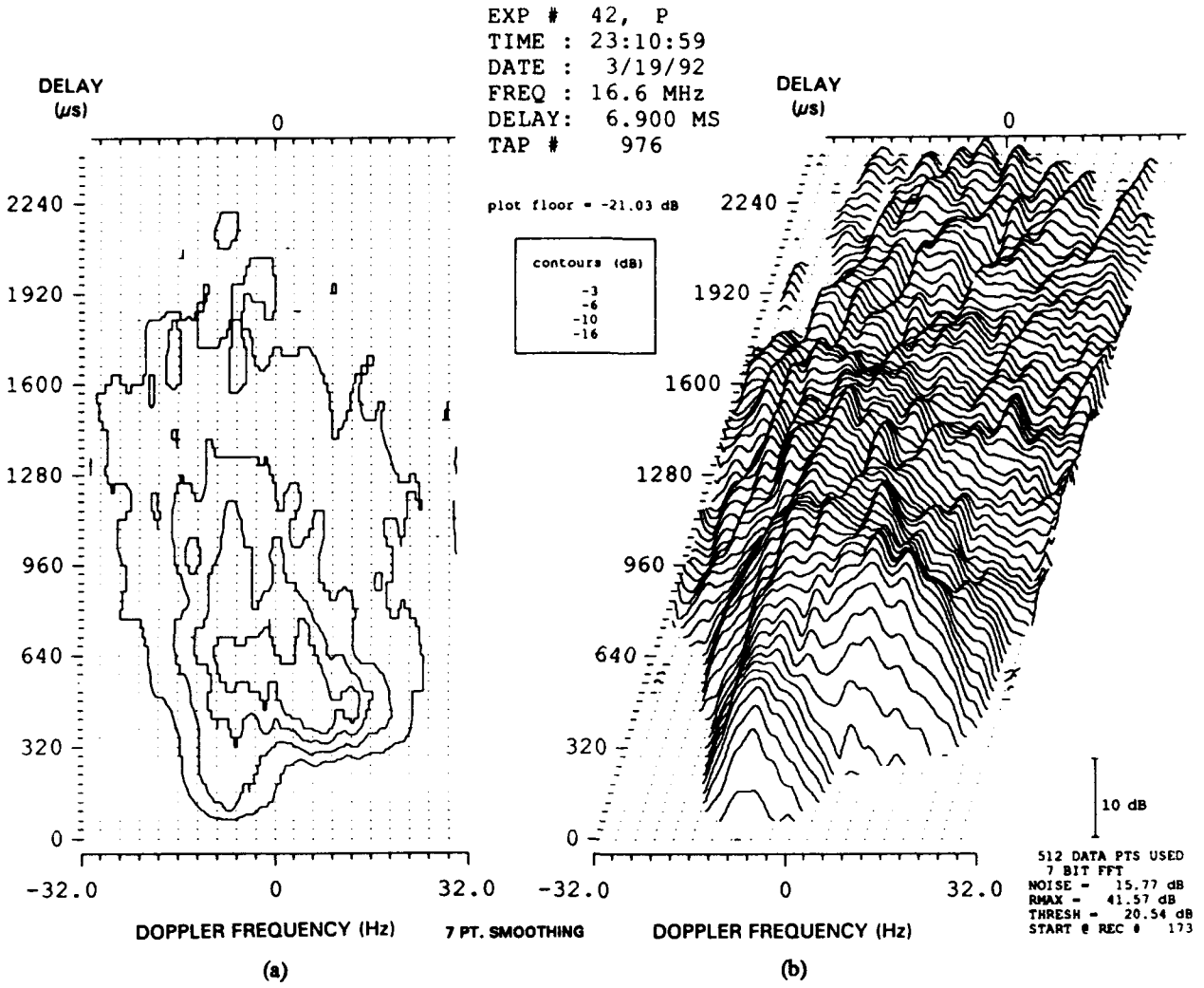

Fig. 17 — Scatter function, 1F2 return, premidnight conditions, K_p = 1, 16.6 MHz, (a) contour plot, (b) 3-D oblique-angle view (origin of delay scale =6.9 ms)

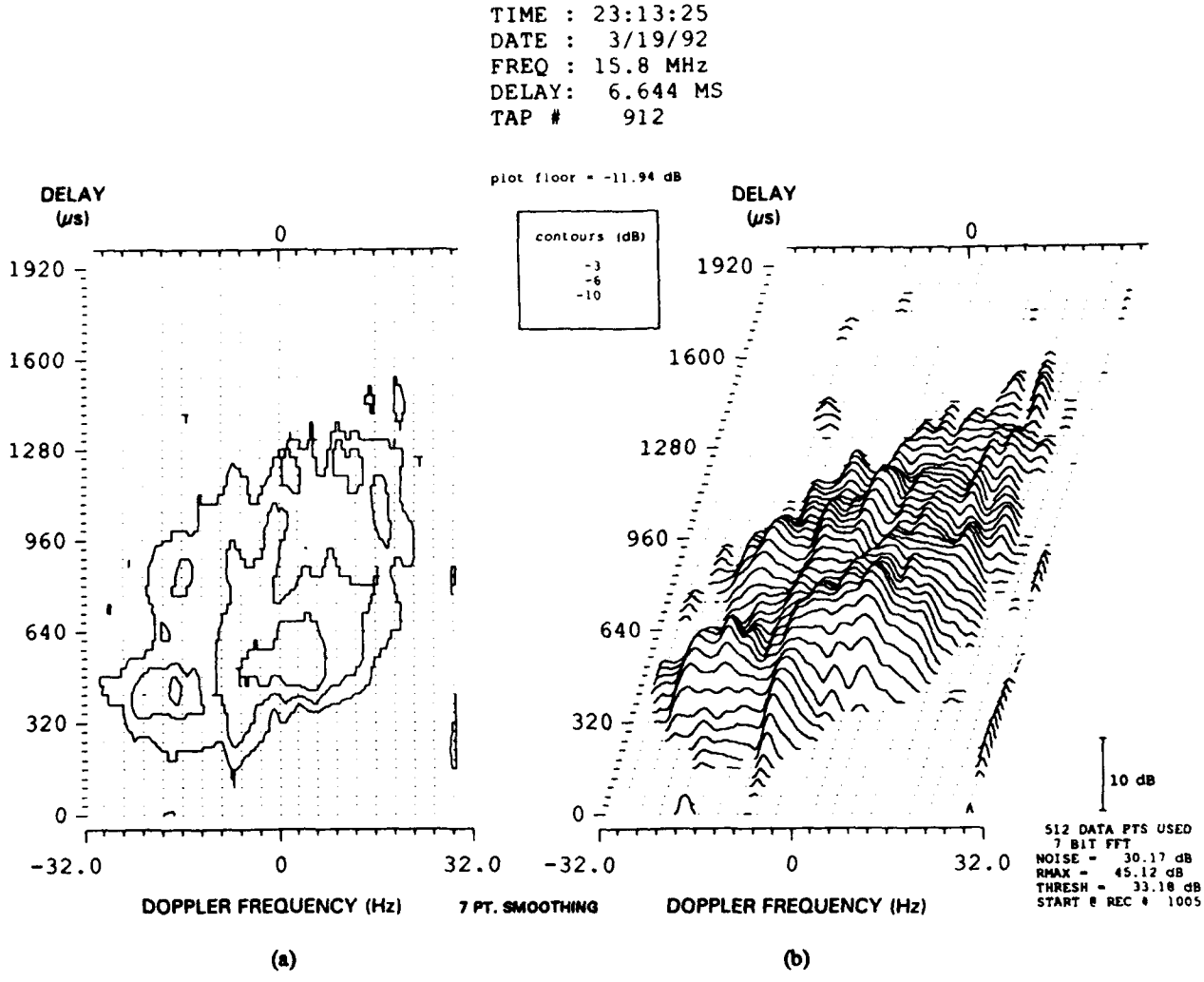

Fig. 18 — Scatter function, 1F2 return, premidnight conditions, K_p = 1, 15.8 MHz, (a) contour plot, (b) 3-D oblique-angle view (origin of delay scale = 6.644 ms)

CASE 6: March 19, 1992; Start Time = 23:37 UT; Exp #43
Probe Frequencies of 16.6 and 15.8 MHz
K_p = 1

Experiment #43 was conducted approximately 30 min after experiment #42 using the same probe frequencies. It has been singled out for detailed scrutiny in this report because it exhibited what appeared to be the broadest combination of delay and Doppler spreads based upon near real-time visual inspection of the data. As in experiment #42, the probing frequencies were well above any identifiable MUF and relied strictly on scatter returns to close the link between transmitter and receiver, as is evident from an inspection of the probe ionogram (Fig. 19). During experiment # 43, scatter signals were observed over the course of the entire 25 min experiment with some apparent waxing and waning caused mainly by fluctuations of background noise and interference. Figures 20, (a) and (b), and 21, (a) and(b), show scattering functions at 16.6 MHz for two times separated by 90 s. In the earlier measurement (Fig. 20) the scattering function appears to be confined to the available Doppler window and is characterized by a mean Doppler shift of 4.2 Hz and by a 2σ Doppler spread of 20.7 Hz. In the later measurement (Fig. 21), the scattering function appears to have shifted to larger values of Doppler shift with the result that some Doppler components extend beyond the upper limit of the Doppler window and are aliassed. For this case, taking appropriate account of the aliassed spectral components, the computed values of mean Doppler shift and 2σ Doppler spread are 12.9 Hz and 20.4 Hz, respectively.

The results at 15.8 MHz are similar to those at 16.6 MHz with the exception that 15.8 MHz was adversely affected by a higher noise and interference background environment as was the case in experiment #42. As a consequence, the plotting threshold on the scattering function diagram is raised and less of the signal is visible. This has a measurable effect on the calculated 2σ Doppler spread as is evident for the two cases shown in Fig. 22, (a) and (b), and Fig. 23, (a) and(b). Figure 22 shows the scattering function for a case in which the level of background noise and interference subsided for a brief interval. The calculated Doppler shift and 2σ Doppler spread for this case are 16.5 Hz and 16.9 Hz, respectively. Fig. 23 illustrates the case of a measurement made 22 s later, when the background noise and interference have returned to a more typical value for this frequency. The calculated Doppler shift and spread for this case are 15.7 Hz and 14.1 Hz, respectively.

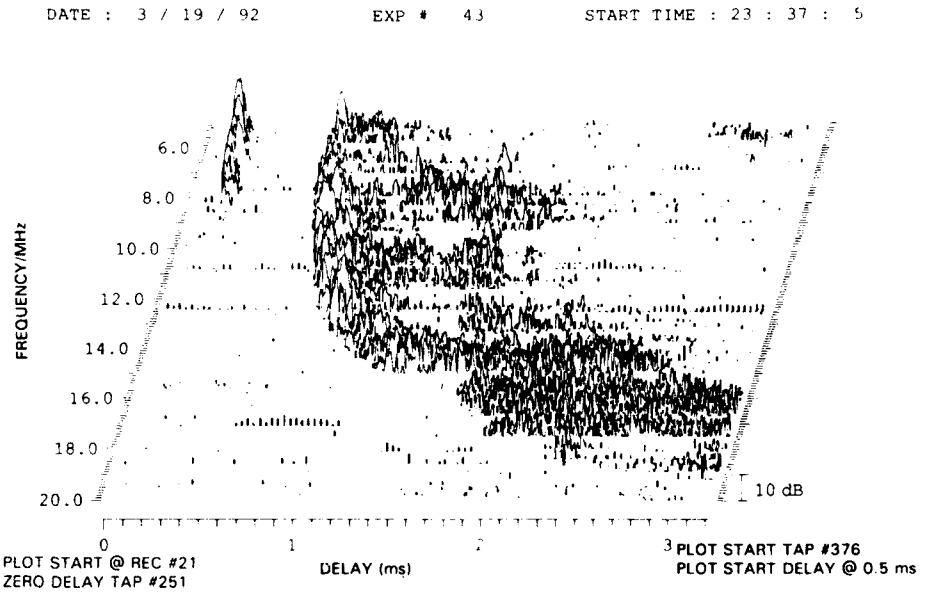

Fig. 19 — Probe ionogram, Sondrestrom to Keflavik, 23:37 UT (origin of delay scale = 4.5 ms)

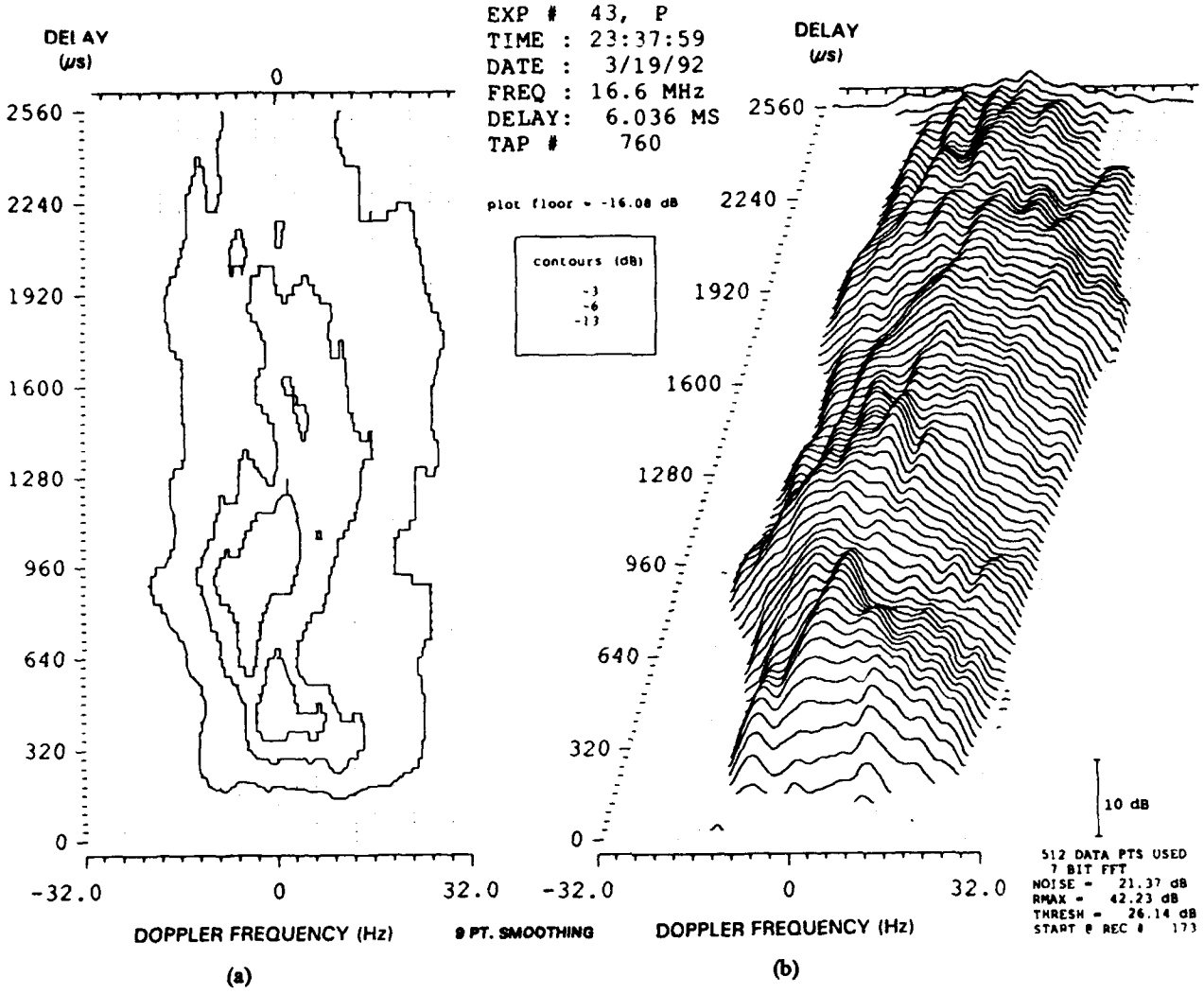

Fig. 20 — Scatter function, 1F2 return, premidnight conditions (23:37:59 UT), K_p = 1, 16.6 MHz, (a) contour plot, (b) 3-D oblique-angle view (origin of delay scale = 6.036 ms)

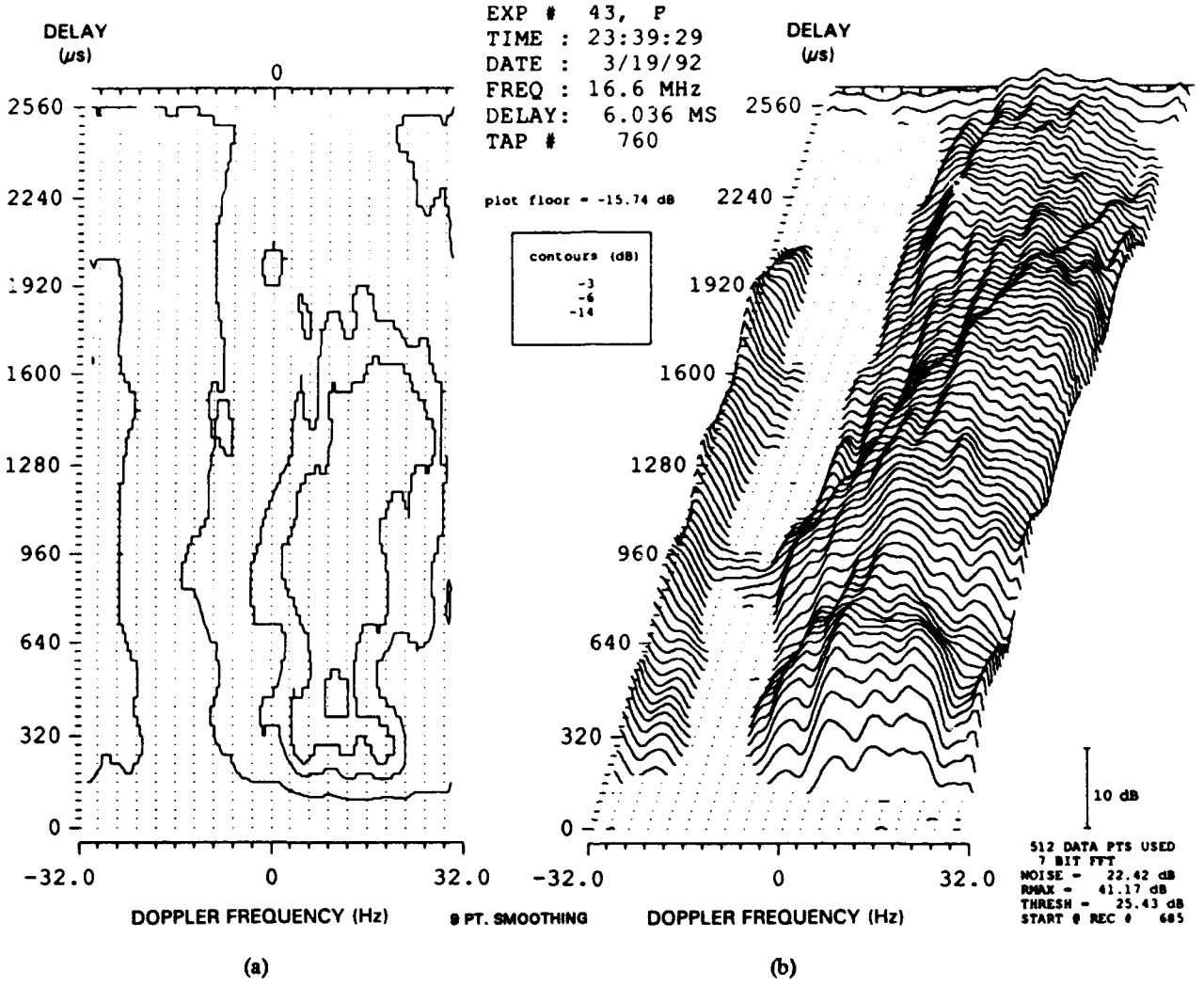

Fig. 21 — Scatter function, 1F2 return, premidnight conditions (23:39:29 UT), K_p = 1, 16.6 MHz, (a) contour plot, (b) 3-D oblique angle view (origin of delay scale =6.036 ms)

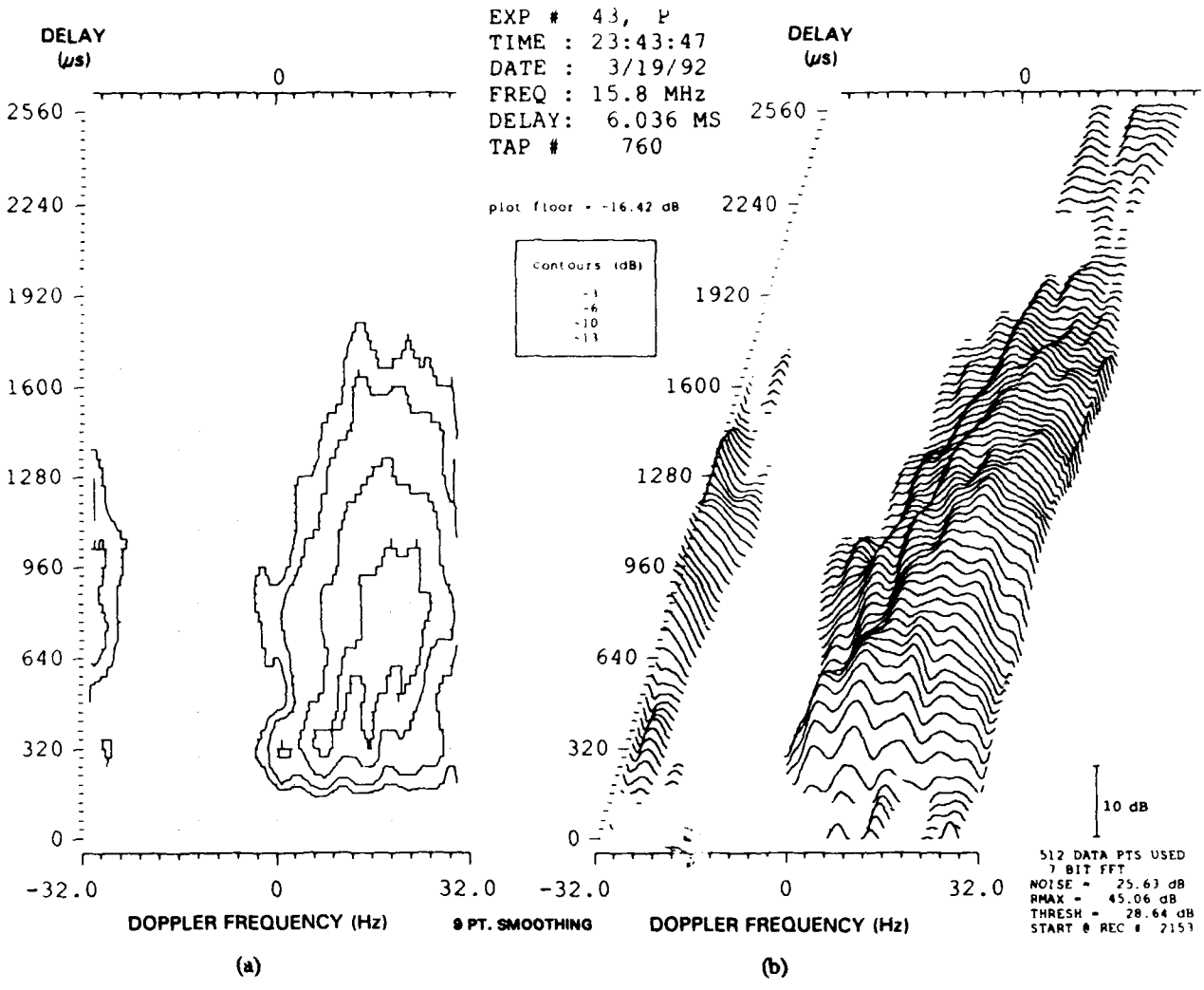

Fig. 22 — Scatter function, 1F2 return, premidnight conditions (23:43:47 UT), SNR = 19.4 dB, Kp = 1, 15.8 MHz, (a) contour plot, (b) 3-D oblique-angle view (origin of delay scale = 6.036 ms)

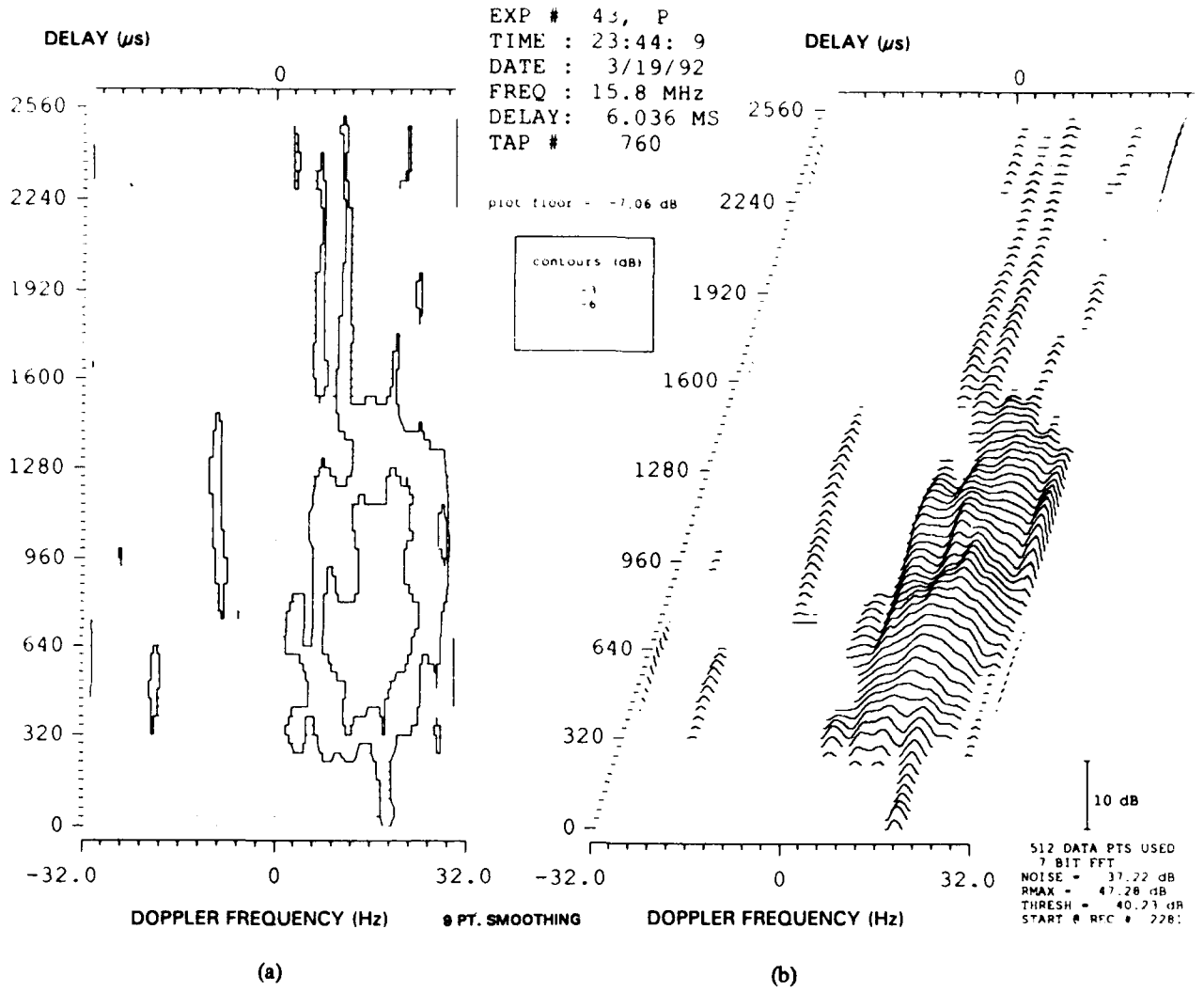

Fig. 23 — Scatter function, 1F2 return, premidnight conditions (23:44:09 UT), SNR = 10.1 dB, K_p = 1, 15.8 MHz. (a) contour plot, (b) 3-D oblique-angle view (origin of delay scale = 6.036 ms)

An important aspect of channel characterization for communication purposes is its time variability. Experiment #43 has been selected to illustrate the variability of the scatter channel by presenting curves of channel characteristics over the course of a 25 min measurement period. These characteristics are presented in Figs. 24, 25, and 26 and summarize the behavior of the channel during the measurement period.

Figure 24 presents curves of signal and noise during the measurement period. Signal is represented by two quantities: (1) the spectral peak of the signal as extracted from the measured scattering function and, (2) the integrated signal power obtained by summing spectral power at all points of the scattering function. The latter quantity would seem to be of significance to an incoherent Rake system that would attempt to sum received signal power. The noise power represented in Fig. 24 is not the same as would be measured in the received pulse response. Instead, it represents the average noise spectral level on the scattering function. The pulse response average-noise level could be obtained by summing the noise spectral components over all Doppler components at each delay. Averaging the result over all delays should provide an accurate measure of the pulse response average noise level. When considering the average noise level measured by the HF channel probe, it should be understood that narrowband interference contributes significantly to the measured value. The signal despreading imposed on received signals tends to convert narrowband signals into broadband signals that, ideally, are then indistinguishable from other uncorrelated wideband signals.

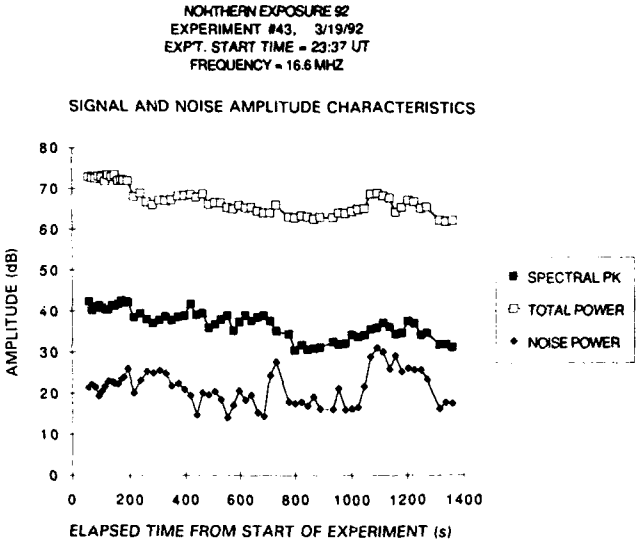

Fig. 24 — Time dependence of signal and noise power, 16.6 MHz, experiment #43 (gain normalized amplitude in dB)

The results shown in Fig. 24 show a gradual decline in received signal strength over the duration of the experiment. The measured noise over this same period shows a modest decline after approximately 300 s followed by a level period interrupted by two noise peaks that are probably associated with periods of sporadic narrowband interference.

Figure 25 summarizes the delay characteristics of the received signals. The upper curve describes the variation of the mean delay of the signal, in milliseconds, and the lower curve describes the variation of the 2σ delay spread. There is a sudden, small increase of mean delay at about 700 s of elapsed time that is associated with changes in the scattering function described in the following paragraphs. Except for minor perturbations, the delay spread shows a small but steady increase with time.

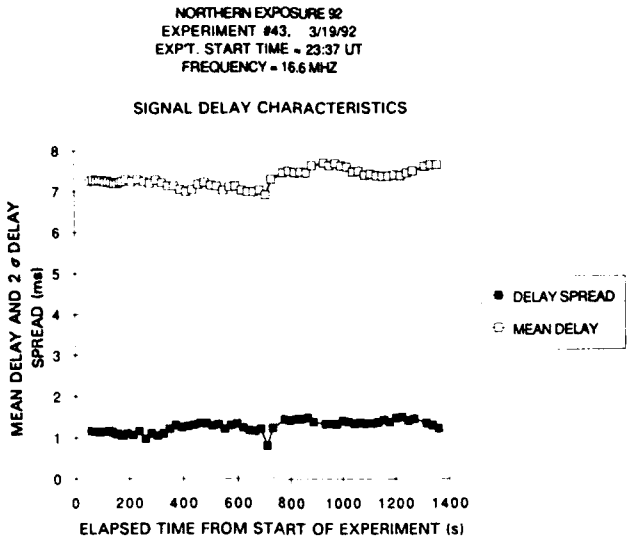

Fig. 25 — Time variation of mean signal delay and 2 σ delay spread at 16.6 MHz, experiment #43

The results of greatest interest are probably those shown in Fig. 26, which summarize the Doppler characteristics of the channel. The curve defined by the unfilled squares shows the slow variation of mean Doppler with time during the experiment. The dark filled squares show the variation of the 2σ Doppler spread over the course of the experiment. During the first 700 s of the experiment, the 2σ Doppler spread of the channel shows a small decline from 20 Hz to 15 Hz. The Doppler spread then rises steeply at 700 s to a value of approximately 30 Hz. Mean Doppler shift of the received signal exhibits a somewhat more complex behavior over the course of the experiment. During the initial 300 s of the experiment, the mean Doppler shift undergoes a steady rise reaching a peak value of 25 Hz at approximately 300 s. Thereafter, the mean Doppler undergoes a slow decline to a minimum value of about 6 Hz at 600 s followed by a steady rise to approximately 14 Hz at 700 s of elapsed time. After 700 s, the Doppler shift declines rapidly to 0 Hz and remains at that value for the duration of the experiment.

As previously mentioned, the motions of irregularity patches and blobs in the nightside auroral and polar regions can be quite complicated. A careful perusal of the sequence of measured scattering functions for experiment #43 reveals that what appears to be a single broad, diffuse scattering function is actually composed of a number of independent elements, and each element is probably related to a distinct irregularity region, which is evolving and moving independently of the others. This scattering function changes shape, amoeba-like, with the result that its mean properties follow no consistent trend. In particular, the behavior of Doppler shift during the first 300 s of experiment time is related to an apparent bulk motion of the scattering function towards positive Dopplers. During the next 300 s, contributions located in the later half of the scattering function move towards negative values of Doppler shift, while the early part of the return remains essentially unchanged.

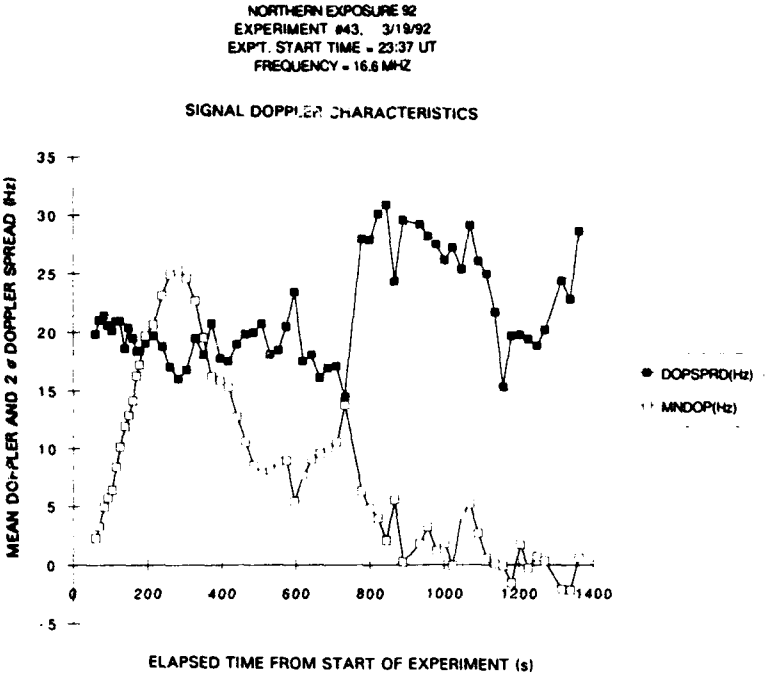

Fig. 26 — Variation of mean Doppler shift and 2 σ Doppler spread at 16.6 MHz, experiment #43

The effect of these uncoordinated changes is to nullify the positive Doppler shift that characterized the early stages of the measurement. Thereafter, the later delay segment of the scattering function develops into a broad dominant feature, simultaneously driving the mean Doppler to 0 Hz and the 2σ Doppler spread to 30 Hz.

6. SUMMARY AND CONCLUSIONS

A cursory review of the data taken on the transauroral channel during the Northern Exposure 92 exercise indicates that one encounters three distinct types of signals on the link between Sondrestrom and Keflavik. These are very strong specularly reflected signals from a laminar ionosphere, specular-multipath signals reflected from large-scale irregularities in a rapidly evolving irregular ionosphere and scatter signals. The specular ionospheric reflections occur during magnetically quiet sunlit conditions, when the ionosphere can be described by a laminar distribution of electron density with height. Specular reflections are limited to frequencies below the MUF for the direct path. The specular-multipath signals are associated with reflection at horizontal gradients of electron density due to the presence of off-path, high-density patches or blobs in a background ionosphere. The specular-multipath signals are also limited to frequencies below a MUF defined by the background ionosphere, the irregularity region electron density distribution, and the path geometry. Scatter signals are observed whenever there are field aligned irregularities of electron density present and when the scatter returns arrive with a delay or Doppler shift that allows their detection in the presence of the much stronger specular returns. In particular, scatter returns are readily observable at frequencies slightly greater than the direct-path MUF for a relatively smooth ionosphere, and at all frequencies greater than the largest MUF for the path when dealing with a spatially-extensive, irregular ionosphere characterized by a general substructure of field aligned irregularities

The spread characteristics of the channel are expected to be most severe during the pre and postmidnight time periods when direct solar effects are minimal and when the effects of electron

precipitation and of transpolar convected high density patches and blobs predominate. This was found to be the case for times between 2200 and 0200 UT. The same behavior may also hold for times after 0200 UT but this could not be confirmed because of locally imposed constraints on our frequencies of operation.

During magnetically quiet ($K_p < 2$) daytime conditions, there is evidence (Wagner and Goldstein, 1990) that the transauroral channel behaves more or less like a regular, daytime, mid-latitude channel. During magnetically unsettled ($2 \leq K_p \leq 3$) daytime conditions, multipath propagation is commonplace especially at frequencies near the MUF (eg., experiments 2 and 4). For these cases, Doppler and delay spreads tend to increase somewhat, but they are well below the extreme values that are usually associated with the transauroral channel. During daytime periods of moderate to severe magnetic disturbance, conditions on the channel change dramatically. It has been demonstrated (Wagner and Goldstein, 1991), and confirmed by other Northern Exposure 92 measurements (Wagner et al., 1993), that moderate magnetic activity of "active" ($3 < K_p < 4$) or "minor magnetic storm" ($4 \leq K_p \leq 5$) intensity can initiate a spread F condition that produces a daytime channel characteristic resembling that of the nighttime channel.

All of the data presented in this report pertain to magnetically quiet conditions ($K_p \leq 2$). Additional Northern Exposure 92 nighttime data are available for which the planetary magnetic activity index K_p reached a value of 4. These data need to be examined to determine the effect, if any, of enhanced magnetic activity on the nighttime spread characteristics of the channel.

The broad delay and Doppler spreads that are observed at night are attributable to scattering from highly anisotropic field aligned irregularities of electron density (slant F echoes) that appear to be a persistent feature of the nighttime F layer. The observed scattering functions appear to be a composite of strong returns from localized regions of elevated electron density and a general background of weaker returns that tend to decrease in amplitude with increasing delay. When the scattering function is dominated by a specular component or by a strong return from a single patch of enhanced electron density, the measured 2σ Doppler spreads tend to be smaller. When, on the other hand, there is no single dominant contributor to the echo power, the spread factors attain their maximum values.

Measured 2σ Doppler spreads ranging between 5 and 30 Hz and 2σ delay spread values between 0.5 and 1 ms were observed regularly at night. The lower values were generally associated with cases where the scattering function was dominated by a single localized feature such as might have been produced by a very strong and discrete irregularity region or by the presence of specular-multipath returns. Lower Doppler spreads ($\sim$ 1 to 2 Hz) and delay spreads (50 to 200 μs) were observed during magnetically quiet daytime conditions at frequencies near the MUF, when multipath was evident on the ionogram at those frequencies. The lowest Doppler and delay spreads were observed during midday when conventional nonspread ionogram traces were visible. For these cases (not selected for detailed discussion in this report) the measured Doppler spread was 0.3 Hz and the measured delay spread was 30 μs, both of which were of the order of the measurement resolution. Finer resolution measurements might have indicated smaller spread values (especially for Doppler spread).

The intensity of the observed slant scatter return relative to that of the specular return ranges in value between ~ -30 dB for the strongest returns and ~ -55 dB* for the weaker scattered returns. Based on previous considerations of the nature of the scattering mechanism, and of the form of the spectral decompostion of the observed ionospheric irregularity regions, it is clear that the strongest scatter returns are received with minimum delay and correspond to scattering from the largest irregularity scale sizes. We therefore attribute echoes received at a level of -30 dB relative to the specular component as

*The lower limit of visibility for these returns is determined by equipment sensitivity.

corresponding to the largest scale sizes. It should be possible, given the required sensitivity, to detect scatter signals many dB below that level from weaker irregularity source regions, or from smaller scale size irregularities received at greater distances from the propagation path.

In assessing the value of the transauroral channel for benchmarking the performance of HF communication modems, it is important to formulate some basis for comparing it with other HF skywave channels. To facilitate this comparison, we have constructed a channel performance map whose ordinate is some measure of received signal amplitude and whose abscissa is the channel spread factor. Two examples of this map are presented in Figs. 27 and 28. In Fig. 27, signal level is represented by the peak spectral amplitude in the scattering function. In Fig. 28, signal amplitude is represented by the incoherent sum of all signal contributions to the scattering function. Both formats are useful for ranking the relative difficulty of different channels provided all measurements are made with the same measurement apparatus and with the same effective radiated power and receive system sensitivity. Benign mid-latitude channels would lie in the upper left-hand corner of either map, while disturbed and highly dynamic channels such as the auroral channel would fall well below and to the right of the benign channels. It should be noted that signal level rather than SNR was used in these comparisons. This was done because it was found that the noise (including the effects of interference) fluctuated widely from one frequency to another.

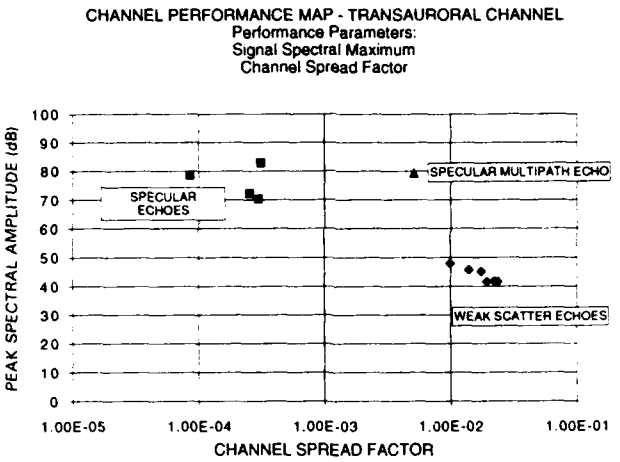

Fig. 27 — Channel performance map, spectral maximum (dB) vs channel spread factor

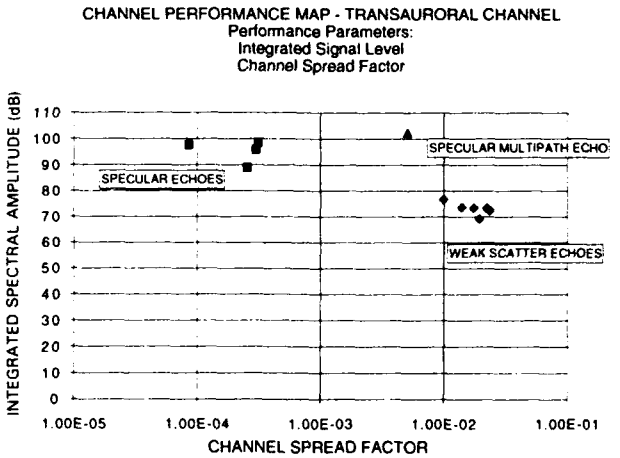

Fig. 28 — Channel performance map, integrated signal (dB) vs channel spread factor

Points plotted on the maps of Figs. 27 and 28 represent specific channels considered in this report and include channels characterized by specular, specular-multipath, and scatter echoes as labelled on the figures. It should be noted that the strongest of the weak scatter echoes are between 25 and 30 dB weaker than the specular echoes in Figs. 27 and 28. Furthermore, the spread factor is approximately two orders of magnitude greater for the scatter channel than for the specular channel. Finally, it needs to be understood that the points, labelled specular echoes in Figs. 27 and 28, actually represent channels measured at times of mild magnetic disturbance (i.e., experiments 2 and 4 for which $K_p = 2$). In addition, they represent frequencies that were very close to the MUF at times when there was extensive multipath near the MUF. The spread factor for these cases is, therefore, probably higher than the one that should be used as the basis for comparison (i.e., the benign, mid-latitude channel). If the delay and Doppler spread values for a midday, benign, mid-latitude channel were used as the reference, the spread factor for the specular components would be at least an order of magnitude smaller than those plotted in Figs. 27 and 28.

The data point representing the specular multipath echo on Figs. 27 and 28 is an interesting hybrid of the specular and scatter cases. It refers to experiment #20 (case 4), which was a nighttime measurement ($\sim$00:01 UT) wherein the probe frequency was below the MUF. There are a few other cases such as this among our measurements but they are not numerous because of restrictions placed on our operations at frequencies below 11 MHz. This case is interesting because the peak spectral amplitude is comparable to that of the cases designated as corresponding to specular reflection, while the spread factor is closer to that of the weak scatter returns. Reference to the ionogram of Fig. 14 makes it obvious that we are dealing with a case of severe spread F and that we are dealing with a highly irregular ionosphere. The value of spread factor for this case is somewhat smaller than that for the other scatter returns however, because of the controlling influence of the specular-multipath echoes in defining the 2σ spread values.

In summary, Fig. 27 shows that scatter signals on the transauroral channel are at least 30 dB weaker than the specular received signals and are characterized by a spread factor that is at least 20 dB greater than that of the reported specular returns. If compared with a benign mid-latitude reference channel, the spread-factor increase of the scatter channel could approach 40 dB. Furthermore, Fig 28 shows that, for an incoherent Rake, the scatter signals tend to be $\sim$20 dB weaker than the reflected signals. Theoretical calculations by Bello (Wagner et al., 1989) indicate that spread conditions such as those observed on the nighttime transauroral channel could require a signal power margin of up to 14 dB over that of an equivalent additive white Gaussian noise (AWGN) channel for a comparable bit error rate. Given the reduced signal level of the nighttime transauroral scatter channel, it seems likely that a power margin of between 14 and 20 dB over that of an equivalent AWGN channel might be required, depending on the Rake's ability to accurately compensate for channel dispersive effects.

7. REFERENCES

Anderson, D.N., J. Buchau, and R.A. Heelis. 1987. "Origin of density enhancements in the winter polar cap ionosphere," 1987 Ionospheric Effects Symposium Conf. Record, 649-657.

Basler, R.P., P.B. Bentley, G.H. Price, R.T. Tsunoda, and T.L. Wong. 1987. "Ionospheric distortion of HF signals," DNA-TR-87-247, 110-119.

Bates, H.F. 1959. "The height of F layer irregularities in the arctic ionosphere," *J. Geophys. Res.*, **64**(9), 1257-1265.

Bates, H.F. 1960. "Direct HF backscatter from the F region," *J. Geophys. Res.*, **65**(7), 1993-2002.

Bello, P.A. 1963. "Characterization of randomly time variant linear channels," *IEEE Trans. on Communication Systems*, **CS-11**(4), 360-393.

Bello, P.A. 1988. "Performance of some Rake modems over the non-disturbed wide band HF channel," MILCOM '88 Conference Record, IEEE, New York.

Booker, H.G. 1956. "A theory of scattering from nonisotropic irregularities with application to radar reflections from the aurora," *J. Atmos. Terr. Phys.*, **8**, 204-221.

Buchau, J., E.J. Weber, D.N. Anderson, H.C. Carlson, J.G. Moore, B.W. Reinisch, and R.C. Livingston. 1985. "Ionospheric structures in the polar cap: Their origin and relation to 250 MHz scintillation," *Radio Sci.*, **20**(3), 325-338.

Feldstein, Y.I. and G.V. Starkov. 1967. "Dynamics of auroral belt and polar geomagnetic disturbances," *Planet. Space Sci.*, **15**, 209-229.

Heelis, R.A. 1982. "The polar ionosphere," *Revs. of Geophys. and Space Phys.*, **20**(3), 567-576.

Knudsen, W.C. 1974. "Magnetospheric convection and the high-latitude F2 ionosphere," *J. Geophys. Res.*, **79**(7), 1046-1055.

Nickisch, L.J. 1992. "Non-uniform motion and extended media effects on the mutual coherence function: An analytic solution for spaced frequency, position, and time," *Radio Sci.*, **27**(1), 9-22.

Peterson, A.M. 1951. "The mechanism of F-layer propagated back-scatter echoes," *J. Geophys. Res.*, **56**(2), 221-237.

Price, R. and P.E. Green. 1958. "A communication technique for multipath channels," Proc. IRE, **46**, 555-570.

Robinson, R.M., R.T. Tsunoda, J.F. Vickrey, and L. Guerin. 1985. "Sources of F region ionization enhancements in the nighttime auroral zone," *J. Geophys. Res.*, **90**(A8), 7533-7546.

Shepherd, R.A. and J.B. Lomax. 1967. "Frequency spread in ionospheric radio propagation," IEEE Trans. Communication Technology, **COM-15**(2), 268-275.

Singh, M., P. Rodriguez, and E.P. Szuszczewicz. 1985. "Spectral classification of medium scale high latitude F region plasma density irregularities," *J. Geophys. Res.*, **90**(A7), 6525-6532.

Spiro, R.W., R.A. Heelis, and W.B. Hanson. 1978. "Ion convection and the formation of the mid-latitude F region ionization trough," *J. Geophys. Res.*, **83**(A9), 4255-4264.

Stein, S. 1987. "Fading channel issues in system engineering," IEEE J. on Selected Areas in Communication, **SAC-5**(2), 68-89.

Tsunoda, R.T. 1988. "High latitude F region irregularities: a review and synthesism," *Revs. of Geophys.*, **26**(4), 719-760.

Wagner, L.S., J.A. Goldstein, and W.D. Meyers. 1987. "Wideband probing of the transauroral channel," MILCOM87 Conference Record, **3**, 876-885, IEEE, New York.

Wagner, L.S., J.A. Goldstein, and W.D. Meyers. 1988. "Wideband probing of the transauroral channel: Solar minimum," *Radio Sci.*, **23**(4), 555-568.

Wagner, L.S., J.A. Goldstein, W.D. Meyers, and P.A. Bello. 1989. "The HF skywave channel: Measured scattering functions for mid-latitude and auroral channels and estimates for short-term wideband HF Rake modem performance," MILCOM89 Conference Record, 830-839, IEEE, New York.

Wagner, L.S., J.A. Goldstein, R.W. Lind, A.Y. Wong, and M.J. McCarrick. 1990. "Channel probe observations of the auroral ionosphere during high-power auroral stimulation experiments," *Radio Sci.*, **25**(6), 1407-1422.

Wagner, L.S. and J.A. Goldstein. 1991. "Response of the high latitude HF skywave channel to an isolated magnetic disturbance," Proc. of fifth international conf. on HF radio systems and techniques, 233-237, IEE, Edinburgh.

Whalen, J.A. 1970. "Auroral oval plotter and nomograph for determining corrected geomagnetic local time, latitude, and longitude for high latitudes in the northern hemisphere," AFCRL-70-0422, Environmental Research Papers No. 327, AD 713170.

Appendix

NORTHERN EXPOSURE 92 EXPERIMENT LOG

NORTHERN EXPOSURE 92 EXPERIMENT SUMMARY SHEET

EXP.	DATE	START TIME (UT)	SEQ. LENGTH CHIPS	NO. FREQS	DELAY RES'N (μs)	EFF. PULSE WIDTH (μs)	DOPPLER WINDOW (Hz)
48	20-Mar-92	20:38:00	255	6	32	32	± 30.64
49	20-Mar-92	21:01:00	255	2	32	32	± 30.64
50	20-Mar-92	22:01:00	255	2	32	32	± 30.64
51	20-Mar-92	23:04:00	255	2	32	32	± 30.64
52	20-Mar-92	23:32:00	255	7	32	32	± 30.64
53	21-Mar-92	0:03:00	255	2	32	32	± 30.64
54	21-Mar-92	1:01:00	255	2	32	32	± 30.64
55	21-Mar-92	2:05:00	255	2	32	32	± 30.64
56	23-Mar-92	21:44:00	255	2	32	32	± 30.64
57	23-Mar-92	22:12:00	255	2	32	32	± 30.64
58	23-Mar-92	22:40:00	255	2	32	32	± 30.64
59	24-Mar-92	1:57:00	255	2	32	32	± 30.64
60	24-Mar-92	2:25:00	255	2	32	32	± 30.64
61	24-Mar-92	2:52:00	255	2	32	32	± 30.64
62	24-Mar-92	20:43:00	255	8	32	32	± 30.64
63	24-Mar-92	21:15:00	255	8	32	32	± 30.64
64	24-Mar-92	21:57:00	255	7	32	32	± 30.64
65	24-Mar-92	23:05:00	255	2	32	32	± 30.64
66	24-Mar-92	23:40:00	255	2	32	32	± 30.64
67	25-Mar-92	22:41:00	255	2	32	32	± 30.64
68	26-Mar-92	15:36:00	255	2	32	32	± 7.66
69	26-Mar-92	15:57:00	255	2	32	32	± 30.64
70	26-Mar-92	16:59:00	255	2	32	32	± 30.64
71	26-Mar-92	17:26:00	255	2	32	32	± 30.64
72	26-Mar-92	18:01:00	255	2	32	32	± 30.64
73	26-Mar-92	18:27:00	255	2	32	32	± 30.64
74	26-Mar-92	18:58:00	255	2	32	32	± 30.64
75	26-Mar-92	19:26:00	255	2	32	32	± 30.64
76	29-Mar-92	18:00:00	255	2	32	32	± 30.64
77	29-Mar-92	18:42:00	255	2	32	32	± 30.64
78	29-Mar-92	19:09:00	255	2	32	32	± 30.64
79	29-Mar-92	20:42:00	255	2	32	32	± 30.64
80	29-Mar-92	22:12:00	255	2	32	32	± 30.64
81	29-Mar-92	23:12:00	255	2	32	32	± 30.64
82	29-Mar-92	23:38:00	255	2	32	32	± 30.64
83	30-Mar-92	19:11:00	255	2	32	32	± 30.64
84	30-Mar-92	19:41:00	255	2	32	32	± 30.64
85	30-Mar-92	22:52:00	255	2	32	32	± 30.64
86	30-Mar-92	23:40:00	255	2	32	32	± 30.64
87	31-Mar-92	0:06:00	255	2	32	32	± 30.64
88	31-Mar-92	0:43:00	255	2	32	32	± 30.64
89	31-Mar-92	22:00:00	255	2	32	32	± 30.64
90	31-Mar-92	22:37:00	255	2	32	32	± 30.64
91	31-Mar-92	23:13:00	255	2	32	32	± 30.64
92	31-Mar-92	23:55:00	255	2	32	32	± 30.64
93	1-Apr-92	1:27:00	255	1	32	32	± 30.64
94	1-Apr-92	21:52:00	255	2	32	32	± 30.64

NORTHERN EXPOSURE 92 EXPERIMENT SUMMARY SHEET

EXP.	DATE	START TIME (UT)	SEQ. LENGTH CHIPS	NO. FREQS	DELAY RES'N (μs)	EFF. PULSE WIDTH (μs)	DOPPLER WINDOW (Hz)
1	13-Mar-92	17:20:00	255	2	4	32	± 2.19
2	13-Mar-92	17:57:00	2047	2	0.5	4	± 2.18
3	13-Mar-92	18:30:00	2047	2	4	4	± 7.63
4	13-Mar-92	19:00:00	255	2	32	32	± 7.66
5	13-Mar-92	19:35:00	255	2	32	32	± 7.66
6	14-Mar-92	20:31:00	2047	2	0.5	4	± 2.18
7	14-Mar-92	21:04:00	2047	5	0.5	4	± 2.18
8	14-Mar-92	21:33:00	255	2	0.5	4	± 2.19
9	14-Mar-92	22:01:00	255	8	32	32	± 7.66
10	14-Mar-92	22:39:00	255	2	32	32	± 7.66
11	14-Mar-92	23:10:00	255	7	32	32	± 7.66
12	14-Mar-92	23:35:00	255	2	32	32	± 7.66
13	15-Mar-92	0:10:00	255	8	32	32	± 7.66
14	15-Mar-92	0:31:00	255	2	32	32	± 7.66
15	15-Mar-92	1:04:00	255	6	32	32	± 7.66
16	15-Mar-92	1:31:00	255	2	32	32	± 7.66
17	15-Mar-92	22:31:00	255	2	32	32	± 30.64
18	15-Mar-92	23:01:00	255	2	32	32	± 30.64
19	15-Mar-92	23:33:00	255	7	32	32	± 30.64
20	16-Mar-92	0:01:00	255	2	32	32	± 30.64
21	16-Mar-92	0:30:00	255	8	32	32	± 30.64
22	16-Mar-92	1:01:00	255	2	32	32	± 30.64
23	16-Mar-92	1:30:00	255	8	32	32	± 30.64
24	16-Mar-92	21:11:00	255	2	32	32	± 30.64
25	16-Mar-92	21:48:00	255	7	32	32	± 30.64
26	16-Mar-92	22:09:00	255	2	32	32	± 30.64
27	16-Mar-92	22:40:00	255	8	32	32	± 30.64
28	16-Mar-92	23:01:00	255	2	32	32	± 30.64
29	17-Mar-92	11:45:00	255	6	32	32	± 30.64
30	17-Mar-92	12:31:00	255	2	32	32	± 30.64
31	17-Mar-92	13:00:00	255	7	32	32	± 30.64
32	17-Mar-92	13:31:00	255	2	32	32	± 30.64
33	17-Mar-92	14:01:00	255	2	32	32	± 30.64
34	17-Mar-92	14:31:00	255	2	32	32	± 30.64
35	17-Mar-92	15:06:00	255	8	32	32	± 30.64
36	17-Mar-92	15:31:00	255	2	32	32	± 30.64
37	17-Mar-92	16:01:00	255	2	32	32	± 30.64
38	19-Mar-92	21:21:00	255	5	32	32	± 7.66
39	19-Mar-92	21:40:00	255	2	32	32	± 30.64
40	19-Mar-92	22:12:00	255	6	32	32	± 30.64
41	19-Mar-92	22:31:00	255	2	32	32	± 30.64
42	19-Mar-92	23:10:00	255	2	32	32	± 30.64
43	19-Mar-92	23:37:00	255	2	32	32	± 30.64
44	20-Mar-92	0:08:00	255	8	32	32	± 30.64
45	20-Mar-92	0:36:00	255	2	32	32	± 30.64
46	20-Mar-92	1:08:00	255	7	32	32	± 30.64
47	20-Mar-92	1:31:00	255	2	32	32	± 30.64

NORTHERN EXPOSURE 92 EXPERIMENT SUMMARY SHEET

EXP.	DATE	START TIME (UT)	SEQ. LENGTH CHIPS	NO. FREQS	DELAY RES'N (μs)	EFF. PULSE WIDTH (μs)	DOPPLER WINDOW (Hz)
95	1-Apr-92	22:25:00	255	2	32	32	± 30.64
96	1-Apr-92	22:57:00	255	1	32	32	± 30.64
97	2-Apr-92	1:10:00	255	1	32	32	± 30.64